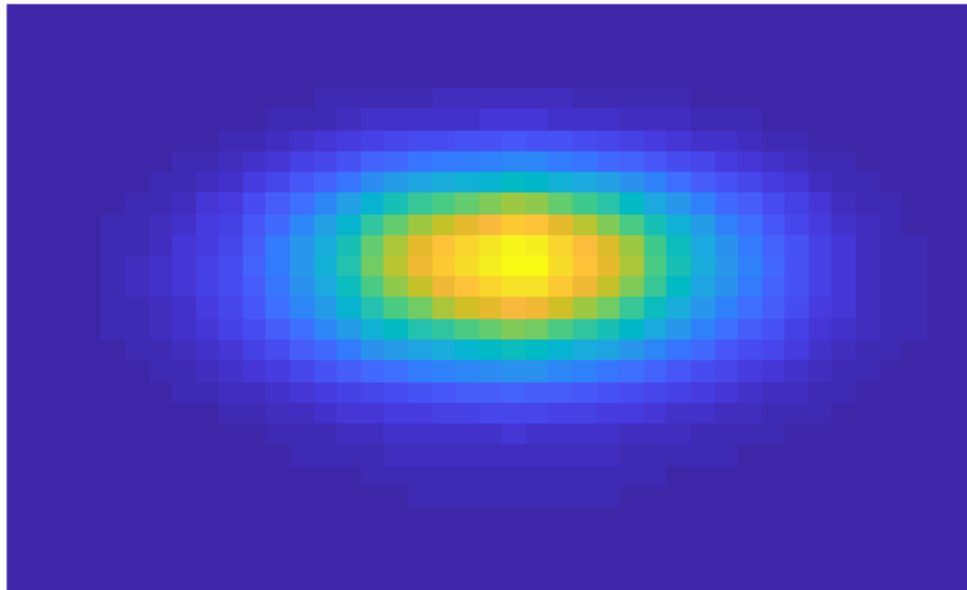




CHALMERS
UNIVERSITY OF TECHNOLOGY



Compact X-FROG for characterisation of ultrafast laser pulses

Broadband-ready X-FROG

Master's thesis in Wireless, Photonics and Space Engineering

Christoffer Krook

MASTER'S THESIS 2019

Compact X-FROG for characterisation of ultrafast laser pulses

Broadband-ready X-FROG

CHRISTOFFER KROOK



CHALMERS
UNIVERSITY OF TECHNOLOGY

Department of Microtechnology and Nanoscience

Division of Division name

Name of research group (if applicable)

CHALMERS UNIVERSITY OF TECHNOLOGY

Göteborg, Sweden 2019

Construction and implementation of a SFG-XFROG ready for broadband pulse
characterisation
CHRISTFFER KROOK

© CHRISTOFFER KROOK, 2019.

Supervisor: Valdas Pasiskevicius, Laser physics, Royal Institute of Technology
Examiner: Victor Torres-Company, Microtechnology and nanoscience, Chalmers
University of Technology

Master's Thesis 2019
Department of Microtechnology and nanoscience
Photonics laboratory
Chalmers University of Technology
SE-412 96 Gothenburg
Telephone +46 31 772 1000

Cover: An interpolated 32×32 SFG-XFROG trace.

Typeset in L^AT_EX
Printed by Chalmers Reproservice
Gothenburg, Sweden 2019

Construction and implementation of a SFG-XFROG ready for broadband pulse characterisation

CHRISTOFFER KROOK

Microtechnology and nanoscience

Chalmers University of Technology

Abstract

This thesis shows the process of constructing a set-up for characterising femto-second laser pulses with which the ultrafast laser physics research group at the Royal Institute of Technology will perform research in the field of ultrafast non-linear optics. In this thesis previous and current methods of femto-second pulse characterisation is described after which the reader is introduced to the implementation and verification of a set-up for performing *Cross-Correlation Frequency-Resolved Optical Gating* (X-FROG). The set-up is demonstrated to successfully characterise the amplitude and temporal width of incident pulses from a Ti:Sa laser oscillator producing roughly 250fs pulses at 800nm. Due to erroneous spectrometer measurements the bandwidth and phase of incident pulses are currently retrieved incorrectly. By locating and fixing the source of the erroneous measurements full characterisation should be successfully performed for femto-second laser pulses. This is further reinforced with simulations. With this set-up successfully implemented in the laser physics groups lab, further research into ultrafast non-linear optics can be performed more easily than before.

Keywords: LASER, FROG, X-FROG, SHG, NONLINEAR OPTICS, SPECTROGRAM.

Acknowledgements

A lot of people have been involved in me getting my masters degree. During the course of these last five years I have learned a lot about my self and I have also grown as a person, entering my studies as a lost young boy and emerging on the other side as a somewhat more grown up 'almost-adult'. I'd like to thank my girlfriend Frida for sticking by me during these years, pretending to be interested when i talk about things surrounding what i do and love. For the same reason I'd like to thank my twin Robert for pretending to listen and letting me pretend to listen when you talk about your own issues and studies. On top of these two people i have my extended family and friends to thank for support and encouragement throughout this process. My close friends from university also deserves their thanks, giving me warm friendship and interesting discussions daily surrounding everything between the earth and the moon. My supervisor Valdas Pasiskevicius deserves his thanks for letting me fine-tune my photonics knowledge and for supporting me through my thesis project and for his help. From KTH I'd like to thank the entire Laser Physics research group for giving me such a great time there and my officemates Anne-Lise, Cherrie and Robert deserves extra thanks for a lot of help with the project and for a warm and nice office climate.

Christoffer Krook, Göteborg, June 2019

Contents

List of Figures	xi
List of Tables	xiii
1 Introduction	1
1.1 Motivation	2
1.2 Difference among ultrafast pulse characterisation techniques	2
2 Theory	3
2.1 laser pulses	3
2.1.1 Dispersion	6
2.2 Nonlinear optics	7
2.2.1 Phase-matching	8
2.3 Measuring of femto-second pulses (preliminary)	10
2.3.1 Autocorrelator	10
2.3.2 Frequency-Resolved Optical Gating	13
2.3.3 Cross-Correlation Frequency-Resolved Optical Gating	18
2.4 Spider	19
3 Method	21
3.1 Equipment	21
3.1.1 MesaPhotonics FROGscan	21
3.1.2 Laser	23
3.1.3 Optical platform	23
3.1.4 Delay-stage	23
3.1.5 Parabolic mirrors	25
3.1.6 Nonlinear crystal	25
3.1.7 Spectrometer	26
3.2 Construction	27
3.3 Software	28
3.3.1 LabVIEW	29
3.3.2 Matlab	31
4 Results	35
4.1 SHG-FROG	35
4.2 X-FROG	39

5 Conclusion	43
Bibliography	45
A Appendix 1	I
A.1 LabVIEW program	I
A.2 Matlab-code	II
A.2.1 FROG-trace simulation	II
A.2.2 UNFROG - returns trace to outer product	II
A.2.3 INTENSITY-REPLACE - applies intensity constraint	III
A.2.4 GET-TRACE - accepts LabVIEW results file and returns spec- trogram	III
A.2.5 GET-PARAMS - accepts pulse as input and returns chirp, bandwidth and tbp	IV
A.2.6 PCGPA - principal components generalized projections algo- rithm	V

List of Figures

2.1	Gaussian, Lorentzian and sech^2 envelope functions	4
2.2	Real part of the Gaussian electric field and its amplitude	5
2.3	Instantaneous frequency with different chirps	5
2.4	Autocorrelator measurement set-up	11
2.5	Autocorrelator measurement for different time-delays. For each plot the orange pulse is time-delayed further	11
2.6	Interferometric autocorrelator	12
2.7	Simulated interferometric autocorrelation trace	13
2.8	General Frequency-Resolved Optical Gating	14
2.9	Visualisation and simulated sample spectrogram	14
2.10	PG-FROG set-up	15
2.11	SD-FROG set-up	16
2.12	Simulated FROG-traces of positively and negatively chirped pulses. a) and b) shows traces for PG-FROG, c) and d) shows for SD-FROG and e) and f) shows for SHG-FROG	18
2.13	Cross-Correlation Frequency-Resolved Optical Gating. BBO stands for Beta Barium Borate which is the nonlinear medium chosen for this application	19
3.1	Inside of the FROGscan. Dark rectangle along the bottom is a plat- form upon which the top-cover rests. RR = Retro Reflector, BS = Beam Splitter	22
3.2	Spectra-physics Tsunami Ti:Sa-laser	23
3.3	The MTS25-Z8 - 25 from Thorlabs.	24
3.4	KDC101 controller. Image from [41]	25
3.5	Spectrometer used	27
3.6	Picture and topological sketch of final set-up	29
3.7	Flowchart of the LabVIEW programs functionality	30
3.8	LabVIEW-interface of the frog-software	30
3.9	Iterative process, image from [5]	32
3.10	Construction of simulated FROG trace. Arbitrary units	33
4.1	Normalised measured and reconstructed trace from the constructed set-up	36
4.2	Difference between measured and reconstructed trace. Reconstructed phase correspond to a FROG error $G = 0.006$	36

List of Figures

4.3	Reconstructed pulses from SHG-FROG measurements	37
4.4	Average pulse with phase and gaussian fit	38
4.5	Measured SHG-FROG trace and raw spectrum	38
4.6	Fundamental harmonic spectrum	39
4.7	Measured FROG and X-FROG traces	40
4.8	Results of X-FROG algorithm provided simulated SFG-XFROG fields	41
A.1	Establishing of spectrometer connection	I
A.2	Updating delay-stage position	I

List of Tables

2.1	Comparison of different FROG set-ups [32]	17
3.1	Parameters for the commercial FROG	21
3.2	Parameters for the MTS25-Z8 - 25 - delay-stage [41]	25
3.3	Parameters for the AvaSpec-Mini2048CL-UVI25 spectrometer [45]. Sensitivity given in counts per μW per seconds integration time. . . .	26
4.1	Results from 5 consecutive FROG measurements	37
4.2	X-FROG results	40

1

Introduction

Characteristics of pulsed lasers makes them suitable for use in a variety of different industrial applications as well as science. In the industry ultrashort laser pulses are used for both micro- and macro-machining [1] as well as for optical communication systems [2]. Scientific applications include: ultrafast spectroscopy, frequency metrology [2, section 1.1] as well as bio-medical applications in for example guided tissue growth and laser eye surgery [3, 4].

As will be made clear in this thesis, the characteristics of these pulses have a major impact on pulse parameters such as peak power, phase and amplitude modulation which might be acquired in optical systems. The measurement and characterisation of these pulses are therefore of great importance.

Several methods have been developed before, with different strengths and weaknesses. One of the earliest methods was the method of *autocorrelation*, with which a rough estimate of the temporal pulse duration could be retrieved [5]. Further methods have been developed from this method of autocorrelation and one successful contender is *frequency-resolved optical gating* (FROG), which allows for the full retrieval of both amplitude and phase of the unknown signal pulse [2]. One of today's most sensitive implementations of FROG is called *cross-correlation frequency-resolved optical gating* (X-FROG), which involves using an already characterised reference pulse to allow for the measurement of weaker pulses [6].

This thesis begins by presenting the underlying theory behind ultrashort laser pulses, nonlinear optics as well as the working principles behind FROG/X-FROG in chapter 2. Chapter 3 presents the reader to the method and implementation carried out during the course of this experiment. In chapter 4 the reader will find the results obtained and lastly chapter 5 will present the conclusions drawn from this thesis work.

1.1 Motivation

The work in this thesis has been carried out at, and for, the department for Laser Physics at the Royal Institute of Technology (KTH). The department performs a lot of research related to lasers within a variety of different fields, and work a lot with femto-second lasers [7]. These laser pulses can not be measured by conventional means such as photo diodes but more creative methods are required. A lot of the research conducted at the department requires either characterising the resulting pulses from experiments or the pulses incident into experiments to properly evaluate results, and as such this means that a device for characterising these pulses is needed [7, 8]. This means that the purpose of this thesis is the construction of a set-up which is to be able to characterise possibly weak pulses and broadband pulses, previous experiments show that in some cases even octave-spanning pulses have been generated in experiments at KTH[7]. The scientific motivation of performing this research at KTH is the possible applications of ultrashort, broadband laser pulses. In for example spectroscopy broadband means that a wider range of frequencies can be investigated, and ultrashort pulses are needed for measuring short events on the same timescale as the pulse duration. With the correct implementation, FROG/XFROG is the state of the art in ultrashort pulse characterisation with the method being implemented in over 10 000 laboratories [9].

1.2 Difference among ultrafast pulse characterisation techniques

Two main families of ultrashort pulse characterisation techniques exist, one being FROG type characterisations and the other involving spectral interferometry [10], namely *spectral phase interferometry for direct electric-field reconstruction* (SPIDER). When SPIDER and FROG were introduced, SPIDER's retrieval algorithm converged much quicker. The time for FROG to converge today has been shown to be less than what is required to plot an extracted pulse, so convergence time is no problem [11, 12]. Furthermore, SPIDER relies on shear-wave mixing by mixing two delayed samples of the pulse with another copy broadened by dispersion. This works with some assumptions. One has to assume that the dispersion is known and that the phase modulation is the same for different intensities.

Experiments at KTH have been shown to produce both complex and/or high time-bandwidth product signals, and as such FROG/XFROG was considered to be the sensible choice as it requires no initial field assumptions and has a 100% convergence rating if implemented correctly [13, 14].

2

Theory

2.1 laser pulses

The word LASER stands for *Light Amplification by Stimulated Emission of Radiation* [15]. A laser provides the user with a source of spatially and temporally coherent light.

Light is classically described well with the help of Maxwell's equations. Deriving the Helmholtz wave equation, an electromagnetic wave is described as [16]

$$\nabla^2 \mathcal{E} - \mu_0 \epsilon_0 \frac{\partial^2 \mathcal{E}}{\partial t^2} = 0 \quad (2.1)$$

where \mathcal{E} is the electric field (V m^{-1}), μ_0 is the magnetic permeability of vacuum (H m^{-1}), ϵ_0 is the electric permittivity of vacuum (F m^{-1}). There are several solutions to this equation, but one frequently used solution is that of a plane wave

$$\mathcal{E}(\vec{r}, t) = A(\vec{r}, t) e^{i(\omega t - \vec{k} \cdot \vec{r})} \quad (2.2)$$

where \vec{k} is the wave number, ω is the radial frequency and \vec{r} is the spatial coordinate vector. From this equation it is clear that the plane wave has both spatial and temporal dependencies which can be separated as $\mathcal{E}(\vec{r}, t) = F(\vec{r}) E(t)$ in the case of a field travelling in a linear medium.

The separation of spatial and temporal components are useful when only one of them are of interest. For the purpose of this thesis emphasis will be on the temporal aspects of laser pulses and thus the spatial component can, for now, be omitted. This new temporal wave can generally be represented as

$$E(t) = C(t) e^{i(\omega t + \phi(t))} \quad (2.3)$$

where $C(t)$ represents a slow-varying envelope and $e^{i(\omega t + \phi(t))}$ represents the carrier wave where $\phi(t)$ is the phase-component.

In theory it is sometimes preferable to represent the envelope with a square pulse, this is never the situation outside of simulation however. The pulse often take the shape of a few select common choices, three of them being the *Gaussian*-, *Lorentzian*- and *sech*²-pulse shapes shown in fig. 2.1 [17].

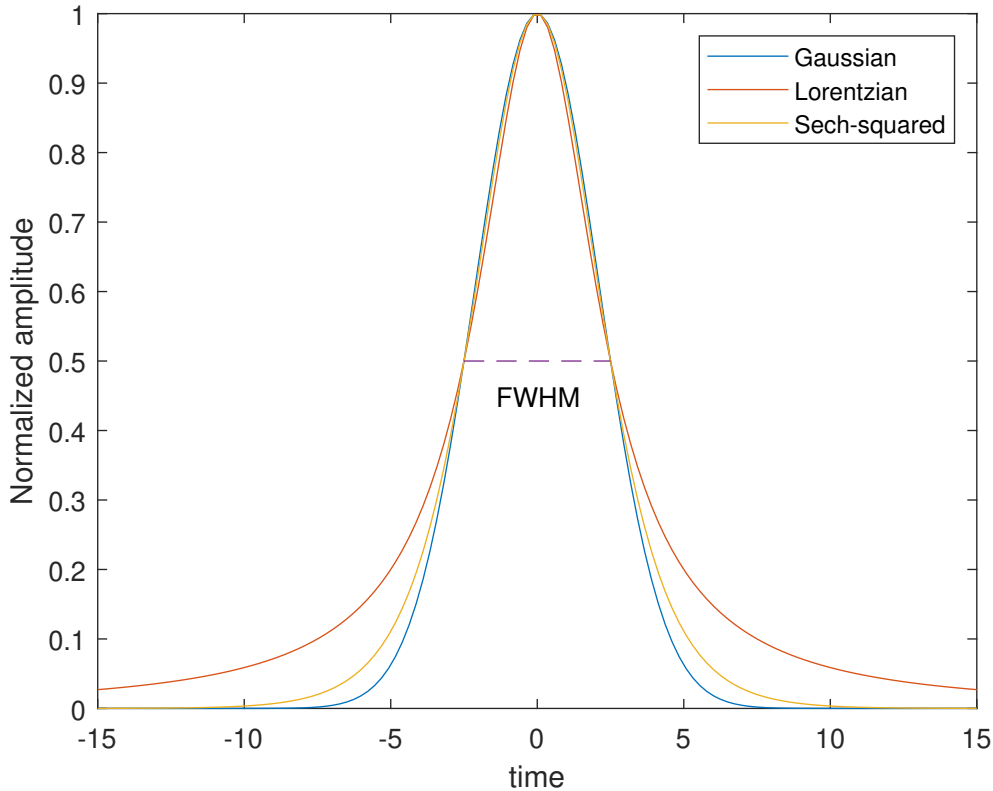


Figure 2.1: Gaussian, Lorentzian and sech^2 envelope functions

They're represented, respectively, as

$$C(t) = e^{-4\log 2\left(\frac{t}{\tau}\right)^2} \quad (2.4a)$$

$$C(t) = \frac{1}{1+p^2}, p = \frac{-t}{\frac{\tau}{2}} \quad (2.4b)$$

$$C(t) = \text{sech}\left(\frac{t}{\frac{\tau}{1.763}}\right) \quad (2.4c)$$

where τ in all of the above represent the *full width at half-maximum* (FWHM). Using eq. (2.3) together with a Gaussian envelope gives a pulse as the one in fig. 2.2.

Just as a pulse has a temporal width τ it also has a spectral width $\Delta\omega$ which can be retrieved by taking the Fourier transform of $E(t)$ to obtain $\hat{E}(\omega)$. The product of these two are referred to as the *time-bandwidth* product (TBP) and is a measure of how spectrally efficient the pulse is [18]. The consequence of this is that for a specific temporal width there exists a lower limit for the spectral width. One of the benefits of using a Gaussian, Lorentzian or sech^2 envelope is that these envelopes minimise the TBP. Such pulses are referred to as *transform-limited*. For example a Gaussian pulse has a minimum TBP of 0.44 and a sech^2 pulse 0.315 [19].

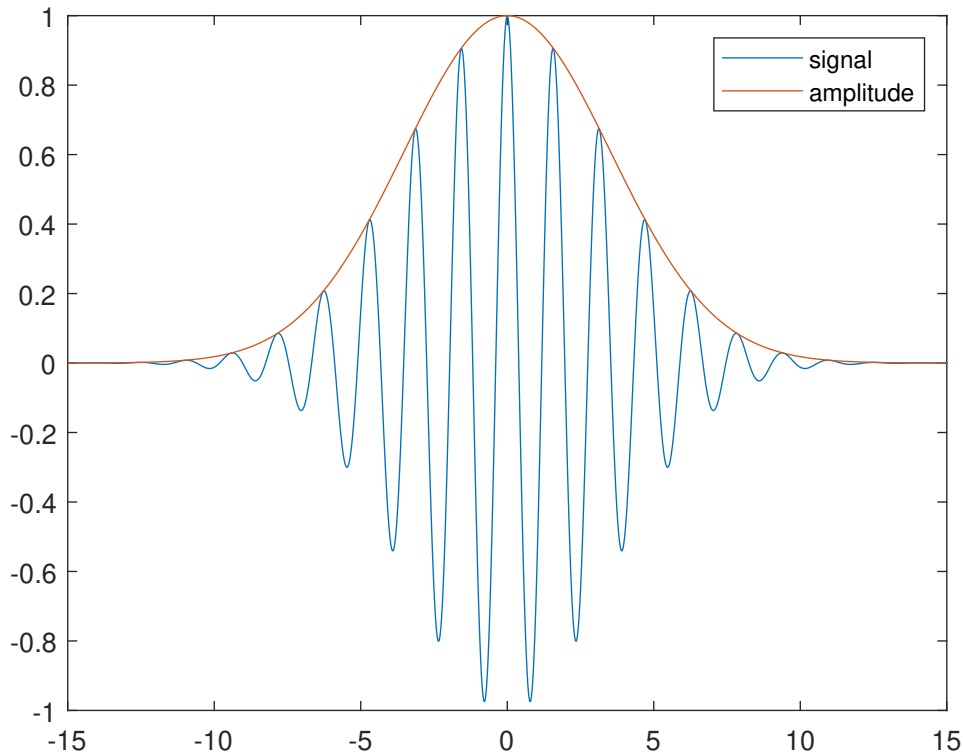


Figure 2.2: Real part of the Gaussian electric field and its amplitude

Another metric for optical pulses is the instantaneous frequency [18, chapter 22]. The instantaneous frequency is the frequency ω_0 at $t = 0$ plus the time-derivative of the phase-component from eq. (2.3)

$$\omega_{\text{instantaneous}} = \omega_0 + \frac{d\phi(t)}{dt} \quad (2.5)$$

Here it is clear that if the phase has a t^2 -dependence the instantaneous frequency will change linearly with time in accordance to $\omega_{\text{instantaneous}} = \omega_0 + \frac{d\phi}{dt} = \omega_0 + \frac{d}{dt}(at^2) = \omega_0 + 2at = \omega_0 + bt$. This property is referred to as a *linear chirp*. In the same manner t^3 -dependent phase will have a quadratic chirp. First order chirps can be seen in fig. 2.3.

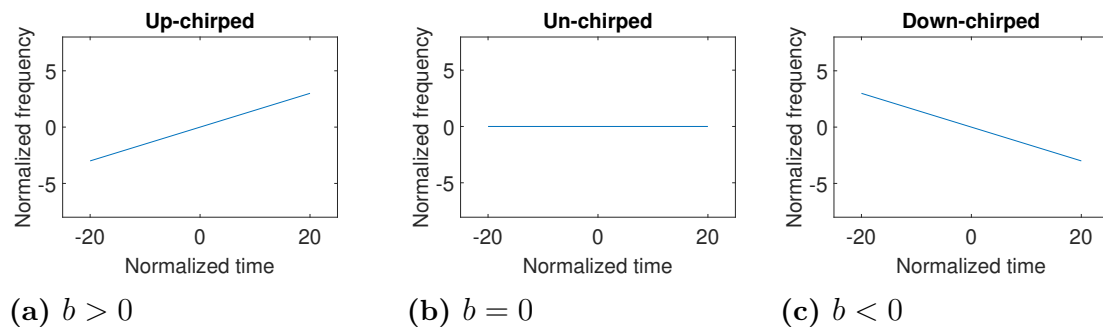


Figure 2.3: Instantaneous frequency with different chirps

The existence of a linear chirp means that the TBP of a pulse will increase [18]. This can be interpreted as the pulse being broader in time than what it needs to be for the given bandwidth. If this is a good or bad thing depends on the application, in for example optical communications it is common to divide the spectrum into individual channels each carrying information. If the number of channels can be increased for the same temporal pulse this means that more data can be sent in a single pulse. Since a pulse is considered transform limited when the TBP is minimised and higher order phase derivatives are zero, the effect of a chirp on a Gaussian pulse for example would be

$$\Delta\nu\Delta\tau_{FWHM} = 0.44\sqrt{1 + b^2} \quad (2.6)$$

where b is the chirp parameter and it is obvious that the temporal FWHM is broadened.

2.1.1 Dispersion

Dispersion is the process of how light at different frequencies propagates through mediums differently. This is a result of a λ -dependent refractive index.

A generalised coordinate independent version of eq. (2.1) is $\nabla^2\mathcal{E} + k^2\mathcal{E} = 0$ in which k is the *wave number* [18]. In the case of 1-D space, a wave with complex amplitude $A = e^{-ikz}$, where z is the distance travelled, will experience a change in phase as it propagates. This wave number can be separated into real and imaginary parts $=\beta - i\alpha$ and the complex amplitude of this wave will now instead appear as $A = e^{\alpha z}e^{-i\beta z}$ where a positive value for α represents absorption in the medium. Most often in the case of free-space optics, the absorption is very small and this part can be neglected for now, and the complex amplitude is thus $A = e^{i\beta z}$ with $\beta = k$.

The properties of β decides how the wave travels through a medium. This β is defined as $\beta(\omega) = \frac{2\pi}{\lambda} = \frac{\omega}{c} = \frac{\omega n(\omega_0 + \Delta\omega)}{c_0}$ and if $\Delta\omega$ is much smaller than ω_0 then this term can be expanded into a Taylor expansion and with higher order terms omitted

$$\beta(\omega) = \beta + \frac{\beta_1}{1!}(\omega - \omega_0) + \frac{\beta_2}{2!}(\omega - \omega_0)^2 + \dots \quad (2.7)$$

where $\beta_i = \frac{d^i\beta}{dt^i}$. For broad spectra, these higher order terms would need to be included as well. If these higher order terms are non-zero, the pulse will behave differently for different frequencies as it propagates [20]. β_1 is related to the *group velocity* of the wave $\frac{1}{\beta_1} = v_g$ and β_1 multiplied with the distance propagated is known as the *group delay*. Further, β_2 represents the *group velocity dispersion* (GVD), a very important parameter, which defines the temporal broadening of a pulse propagating in a media. The relationship between GVD and *dispersion coefficient* is

$$D = -\frac{2\pi c}{\lambda^2}\beta_2 \quad (2.8)$$

[20]. The difference in temporal width of a pulse in such a medium is

$$\delta t = |D_\lambda| \delta_\lambda z \quad (2.9)$$

where z represents the distance travelled through the medium [18]. Thus, having non-zero higher order phase components means that a pulse will not be the same when it arrives at its destination compared to what it was at its origin. The pulse will be either initially broadened or compressed if the pulse is linearly chirped due to the pulse having a linearly varying frequency and the material allowing different spectral components to travel at different velocities.

2.2 Nonlinear optics

Nonlinear optics is the back-bone of this thesis and the theory surrounding it is fundamental in the characterisation of ultra-short laser pulses.

In the previous section the Helmholtz wave equation was used to represent the electric field. This can be further elaborated to include the polarisation component of the electric field as

$$\nabla^2 \mathcal{E}(\vec{r}, t) - \mu_0 \epsilon_0 \frac{\partial^2 \mathcal{E}(\vec{r}, t)}{\partial t^2} = \mu_0 \frac{\partial^2 \mathcal{P}(\vec{r}, t)}{\partial t^2} \quad (2.10)$$

where \mathcal{E} is the electric field (V m^{-1}), c_0 is the speed of light in vacuum (m s^{-1}), (μ_0) is the magnetic permeability in vacuum (H m^{-1}) and \mathcal{P} is the polarisation density [18, chapter 21]. As can be observed here, the wave depends on both the electric field and the polarisation density. A relationship between the two can be defined as

$$\mathcal{P} = \epsilon_0 \chi^{(1)} \mathcal{E} + \mathcal{P}_{NL} \quad (2.11)$$

where the first term on the right hand side represents the linear relationship in the material and the second term represents the nonlinear terms. This second term is preferable expanded as a Taylor series to appear as

$$\mathcal{P}_{NL} = \epsilon_0 (\chi^{(2)} \mathcal{E}^2 + \chi^{(3)} \mathcal{E}^3 + \dots) = \mathcal{P}^{(2)} + \mathcal{P}^{(3)} + \dots \quad (2.12)$$

Here, $\chi^{(i)}$ is the materials susceptibility and these are constants specific to each material. The first term of eq. (2.12) is referred to as the second order non-linearity and the second term is referred to as the third order non-linearity and so forth.

From eq. (2.11) and eq. (2.12) it is obvious that the strength of each non-linearity is related to the incoming fields amplitude. By defining a field with amplitude $A_1(t)$ and frequency ω_1 which can be represented as $E(t) = A_1(t) \cos(\omega_1 t)$ it can be rewritten with Eulers formula as

$$\mathcal{E}(t) = \frac{A_1(t)}{2} (e^{i\omega_1 t} + e^{-i\omega_1 t}) = \frac{A_1(t)}{2} e^{i\omega_1 t} + \text{c.c} \quad (2.13)$$

where c.c stands for complex conjugate [21].

The second order polarisation for this field is according to eq. (2.12) expressed as $\mathcal{P}^{(2)} = \epsilon_0 \chi^{(2)} \mathcal{E}^2$. By plugging eq. (2.13) into this expression the resulting polarisation will be

$$\mathcal{P}^{(2)} = \frac{\epsilon_0 \chi^{(2)}}{4} A_1 A_1 e^{i2\omega_1 t} + \text{c.c}$$

where it can be observed that a frequency component with $\omega = 2\omega_1$ exists. This process is referred to as *second harmonic generation* (SHG).

Similarly, if the electric field $\mathcal{E}(t)$ consists of two separate frequency components $\mathcal{E}(t) = \frac{1}{2}(e^{i\omega_1 t} + e^{i\omega_2 t}) + \text{c.c}$ the resulting second order polarisation would carry components with

$$\omega = 2\omega_1 \textit{ Second Harmonic Generation (SHG)} \quad (2.14a)$$

$$\omega = 2\omega_2 \textit{ Second Harmonic Generation (SHG)} \quad (2.14b)$$

$$\omega = \omega_1 + \omega_2 \textit{ Sum Frequency generation (SFG)} \quad (2.14c)$$

$$\omega = \omega_1 - \omega_2 \textit{ Difference Frequency Generation (DFG)} \quad (2.14d)$$

$$\omega = 0 \textit{ Optical Rectification (DC-Component)} \quad (2.14e)$$

thus nonlinear crystals are suitable for generating a variety of new frequencies [21]. Another nonlinear effect is the change in refractive index due to in an incident DC-field known as the *electro-optic effect* [22]. Potential applications for this effect is modulators and optical switches [20].

2.2.1 Phase-matching

The plane wave in eq. (2.2) shows that the spatial component of this wave is the wave vector \vec{k} and the spatial coordinate vector \vec{r} . The vector

$$\vec{k} = (k_x, k_y, k_z)$$

is the wave vector with a normal in the direction of propagation for the plane wave [18, page 44]. The magnitude of this vector is

$$k = \frac{2\pi}{c} = \frac{\omega n(\omega)}{c_0}$$

In the case of SHG for example, the second order polarisation component carries the frequency $\omega_3 = \omega_1 + \omega_2$ which in turn means that $\lambda_3 = \frac{\lambda_1}{2}$ if $\omega_1 = \omega_2$. This means that the new wave vector is $k_3 = \frac{4\pi n_{\text{medium}}}{\lambda_0}$ from which one can conclude that \vec{k}_3 for the second order polarisation needs to be

$$\vec{k}_3 = \vec{k}_1 + \vec{k}_2 \quad (2.15)$$

which is referred to as the condition for *phase-matching*. Without phase-matching there will be no strong second order polarisation. From this, one important measure can be defined as the *phase-mismatch* $\Delta\vec{k} = \vec{k}_3 - \vec{k}_1 - \vec{k}_2$.

As have been mentioned earlier, strong higher order nonlinear electric fields requires phase-matching, and an increase in phase-mismatch decreases this nonlinear field strength significantly. Due to chromatic dispersion in different optical mediums, different wavelength travels through the medium with different velocities. This means

that, for signals with different group velocities, the phase-mismatch will increase as the field propagates through the nonlinear medium [23]. The effect of this is that, for a desired optical bandwidth and a given nonlinear medium, there is a maximum thickness over which the condition for phase-matching will be satisfied. The same is valid the other way around, for a given nonlinear medium with a given length, a maximum spectral bandwidth for which phase-matching will occur exists.

Consider the case where two incoming fields $E(\omega_1) = E_1 e^{i(\omega_1 t - \vec{k}_1 \cdot \vec{r})}$ and $E(\omega_2) = E_2 e^{i(\omega_2 t - \vec{k}_2 \cdot \vec{r})}$ with $\omega_2 = \omega_1$ are incident on a nonlinear interface. SHG generation will result in the nonlinear field $\mathcal{P}^{(2)} \propto e^{i\vec{k}_3 \cdot \vec{r}} e^{i\Delta\vec{k} \cdot \vec{r}}$ where $\Delta\vec{k}$ is the phase-mismatch. [18] derives that the existence of a phase-mismatch reduces the intensity of the second order nonlinear field by a factor $\text{sinc}(\Delta\vec{k}L/2\pi)$ where L is the length of the nonlinear medium. In the case of a nonlinear crystal this would be referred to as the thickness.

Further, [18] defines the parameter *interaction length* $L_c = 2\pi/|\Delta\vec{k}|$ which is the distance over which the nonlinear interaction is still strong. From this follows that the condition

$$|\Delta\vec{k}(\omega_0 + \Delta\omega)| \leq 2\pi/L$$

defines the spectral band over which this interaction length can occur. If $\Delta\omega$ is small, we can see that, just as in eq. (2.7) this is the first order derivative of a Taylor expansion, $\Delta\vec{k}'\Delta\omega$. The expression is now divided with $|\Delta\vec{k}'|$ and the spectral width over which phase-matching efficiently occurs is

$$\Delta\omega = \frac{2\pi}{|\Delta\vec{k}'|L} \quad (2.16)$$

and the spectral width in Hz is

$$\Delta\nu = \frac{1}{|\Delta\vec{k}'|L} \quad (2.17)$$

where $\beta = k$ and as such the phase-matching bandwidth is

$$\Delta\nu = \frac{1}{2} \left| \frac{L}{\nu_{SHG}} - \frac{L}{\nu_{\omega_1}} \right|^{-1} = \frac{c_0}{2L} \frac{1}{|N_{SHG} - N_{\omega_1}|} \quad (2.18)$$

where N_{SHG} and N_{ω_1} represents the *group index* of the two frequencies. The group index is defined as the ratio between the field velocity in vacuum and the group velocity $N_g = \frac{c_0}{v_g}$.

Another metric for the efficiency of a nonlinear medium is the conversion efficiency. By simple reasoning one can conclude that the length over which nonlinear interaction occurs is related to the magnitude of the resulting nonlinear optical mode. For SHG the conversion efficiency between the SHG-mode and the fundamental mode is given in [18] as

$$\eta_{SHG} = C^2 \frac{L^2}{A} P \quad (2.19)$$

where C is a constant proportional to $\chi^{(2)}$, L is the interaction length, A is the interaction area and P is the incident power. Here again we see the relationship between incident power and SHG-mode strength as the conversion efficiency is proportional to incident power. Interesting to note here however is that the conversion efficiency is proportional to L^2 , which means that a compromise needs to be done between phase-matching bandwidth and sensitivity of SHG as a thinner crystal would increase the phase-matching bandwidth but reduce the conversion efficiency.

2.3 Measuring of femto-second pulses (preliminary)

Today laser pulses are short enough that they far exceed even the fastest photo-detectors available in the pico-second range (1ps = 10^{-12} s) [5], with pulses potentially being as short as a few atto-seconds (1as = 10^{-18} s) [24]. This thesis will mainly focus on femto-second pulses (1fs = 10^{-15} s) which is still beyond what is possible to measure with photo-detectors.

In order to understand how *Frequency-Resolved Optical-Gating* (FROG) works, previous methods must first be described as they build upon each other.

2.3.1 Autocorrelator

In 1967 pulses were already shorter than what could be detected by conventional means, thus a paper was released in the Journal of Applied Physics which proposed a new method to detect the temporal width of such pulses [25]. The method is referred to as the method of *autocorrelation*.

autocorrelation refers to the autocorrelation of a signal with itself. In the simplest case, this can be described as a form of convolution, convolution being defined as

$$(f * g)(t) \triangleq \int_{-\infty}^{\infty} f(\tau) g(t - \tau) d\tau \quad (2.20)$$

which in the case of autocorrelation would take the form

$$\Omega = \int_{-\infty}^{\infty} f(t) f(t + \tau) d\tau \quad (2.21)$$

where the difference is that the functions are the same and that the one that is swept temporally is not time-reversed.

To utilise this in characterisation of ultrafast laser pulses [25] implemented a version of the Michelson-interferometer [18, page 60]. An incoming laser pulse is split using a beam-splitter and then recombined in a nonlinear medium with the possibility to introduce different relative time-delays between the now two pulses approaching the interface. In the situation [25] demonstrated, a KDP-crystal was used to produce SHG. This new SHG-mode is measured with a power meter and the measured

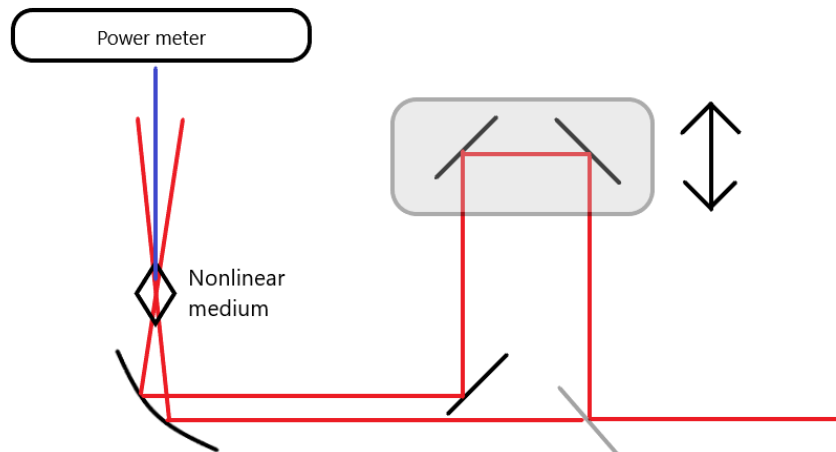


Figure 2.4: Autocorrelator measurement set-up

intensity is plotted vs time-delay of one of the arms to create an autocorrelation plot. The degree to which the pulses are temporally overlapping decide the relative strength of the SHG mode, with $\tau = 0$ providing the strongest signal when temporal overlap is maximised. The set-up itself is shown here in fig. 2.4 and a measurement of a simulated pulse in fig. 2.5.

Autocorrelation and corresponding autocorrelation trace

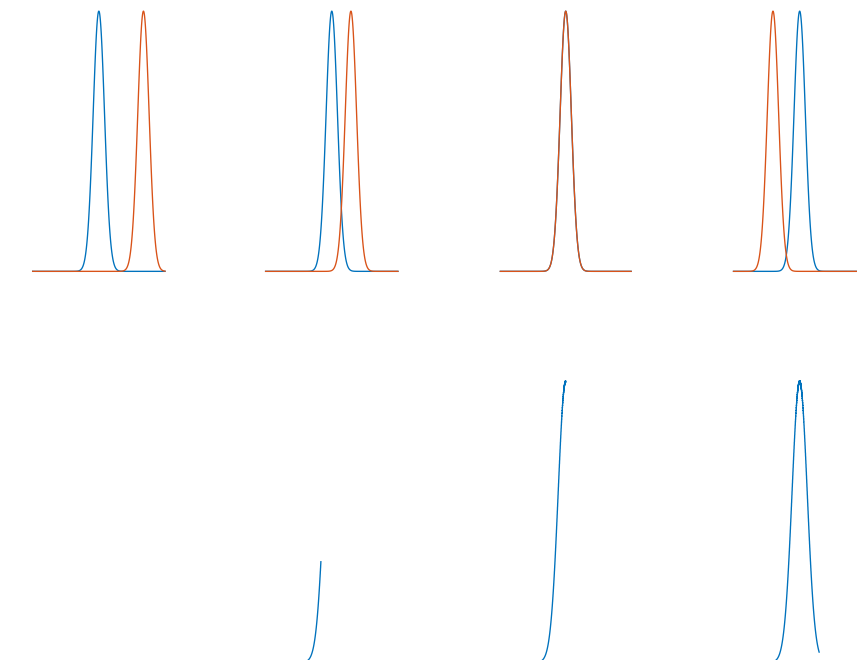


Figure 2.5: Autocorrelator measurement for different time-delays. For each plot the orange pulse is time-delayed further

Due to the mathematics behind the autocorrelation the width of the autocorrelation signal will be larger than the actual pulse width [25]. The width of the measured autocorrelation trace needs to be reduced with a de-convolution factor [2], $\sqrt{2}$ for Gaussian pulses and 1.543 for sech^2 -pulses are two examples. This means that the initial pulse shape needs to be guessed and then an estimated temporal width can be approximated. This and the fact that there is a finite number of measurements and thus a non-infinitesimal time-step some errors and margins are introduced. Unless the resulting trace is interpolated after measuring, the resolution on the final width would be equal to the time-delay step-size. Sharp and symmetrical features in the pulses are removed as well, since the trace is symmetric by definition [2] and thus these features can't be retrieved. A major limitation of autocorrelation however is the simple fact that it can not retrieve the phase of the pulse due to this being a 1-D phase-retrieval problem, which is currently one of mathematics unsolved problems [5]. For a measured intensity, there is an infinite number of signals that would correlate to this intensity.

An alternative version to this method is to implement an *interferometric autocorrelator* [26]. This set-up is in many ways similar to the one in the previously mentioned autocorrelator. The two beams arrive in the crystal through a co-linear setup, meaning that they arrive parallel and superposed, and thus the signal strength in the crystal depends on the variable delay between the pulses. When the two beams are a half wavelength apart there is destructive interference, and there would be no SHG. Similarly, when the variable delay is extended or shortened another half wavelength, the interference is constructive and there is a peak in the signal. This set-up can be seen in fig. 2.6 and a simulated interferometric autocorrelation trace in fig. 2.7.

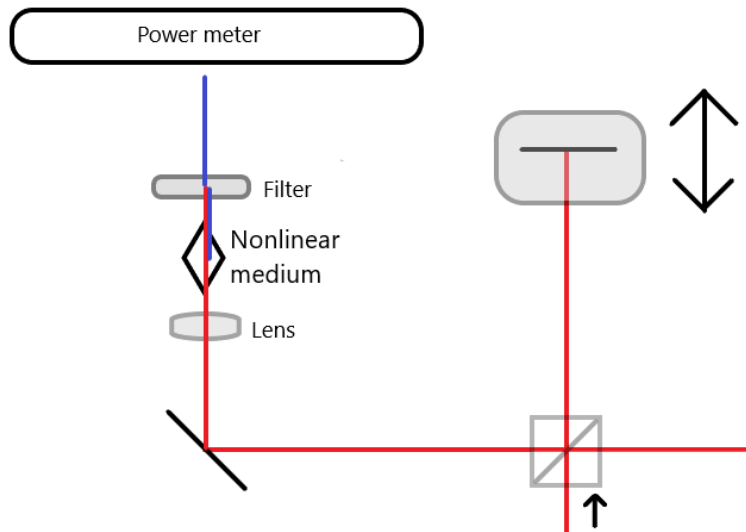


Figure 2.6: Interferometric autocorrelator

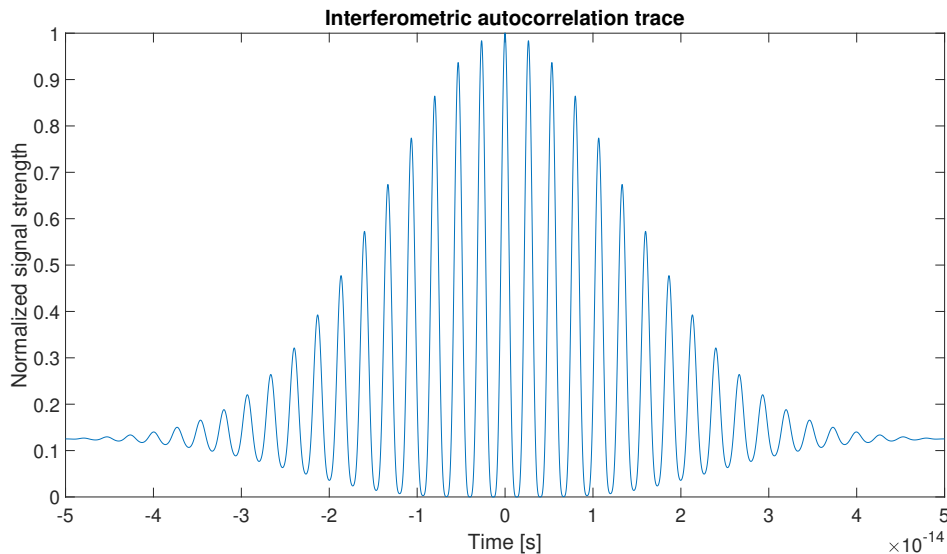


Figure 2.7: Simulated interferometric autocorrelation trace

In this figure a clear pulse shape can be seen, and the width of said signal can be estimated as in the case of autocorrelation. Since this in itself is still an autocorrelation trace, the same broadening previously mentioned is present here as well. Another restriction by interferometric autocorrelation is that care is needed for the situation when the spectrum of the nonlinear-mode contains the spectrum of the fundamental harmonic. This means that when interferometric autocorrelation is done here, it may indicate the presence of a short pulse that is not really there.

2.3.2 Frequency-Resolved Optical Gating

Frequency-Resolved Optical Gating (FROG) is the backbone of this thesis. This method was presented as a solution to overcome the shortcomings of autocorrelation and several different versions and implementations of FROG exists, each with their own strengths and weaknesses.

What makes FROG able to extract the phase of the measured data? The data used in FROG is, as will be made clear, a spectrogram, which is a representation of several spectrums measured at different time-delays τ . These are plotted with frequency on the y-axis and τ on the x-axis and thus a 2-D spectrogram. Extracting an unambiguous signal from a spectrogram is possible due to the fact that retrieving phase and amplitude from a spectrogram is the process of 2-D phase-retrieval, which unlike 1-D phase-retrieval, is a solved mathematical problem.

The fundamental theorem of calculus states that any 1-D polynomial can be factored infinitely [27]

$$f_{N-1}x^{N-1} + f_{N-2}x^{N-2} + \dots + f_0 \quad (2.22)$$

and the existence of this theorem implies that the number of solutions are infinite and unambiguous phase-retrieval is impossible. The fourier magnitude of the measured

signal can be determined but the phase can not. This theorem fails however for 2-D polynomials and thus this implies that a solution exists with but a few trivial ambiguities such as an exponential with a constant phase term for example [27]. As the sample size of the spectrogram grows larger however, these ambiguities become fewer and fewer and as such the solutions are assumed to be unique [5].

In 1993 Trebino, Kane and DeLong proposed the method of FROG for full characterisation of ultrashort laser pulses [28], meaning that both amplitude and phase could be retrieved. In their proposed experiment, the set-up is similar to that of the autocorrelator, but the biggest difference is that the power meter is instead replaced with a spectrometer as in fig. 2.8. This means that for different temporal overlaps between the signal- and the gate-pulse, a spectrum can be measured. These measurements can be stitched together to form a *spectrogram* [29]. A spectrogram is a method of visualising a relationship between frequency and time for a signal, often used in the analysis of acoustics. Examples of suggested and existing applications are visual hearing aids and vocal training [30, 31]. The individual measurements are plotted with time on the x-axis and frequency on the y-axis. Explanation of the spectrogram and sample FROG-trace can be found in fig. 2.9.

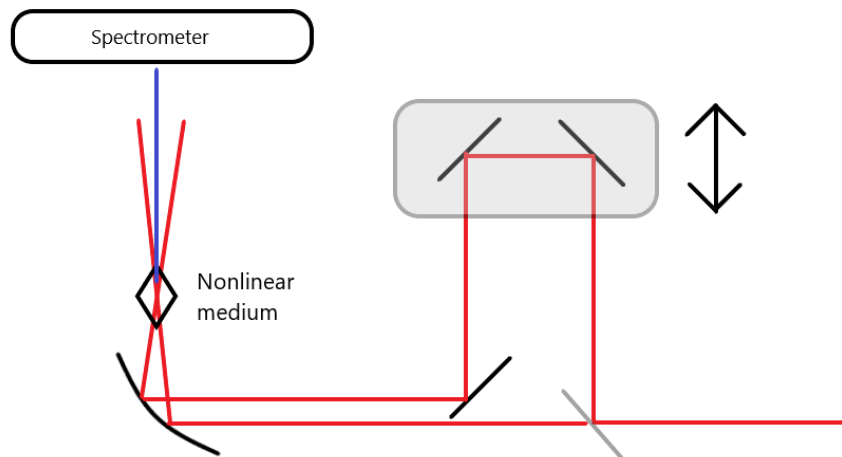


Figure 2.8: General Frequency-Resolved Optical Gating

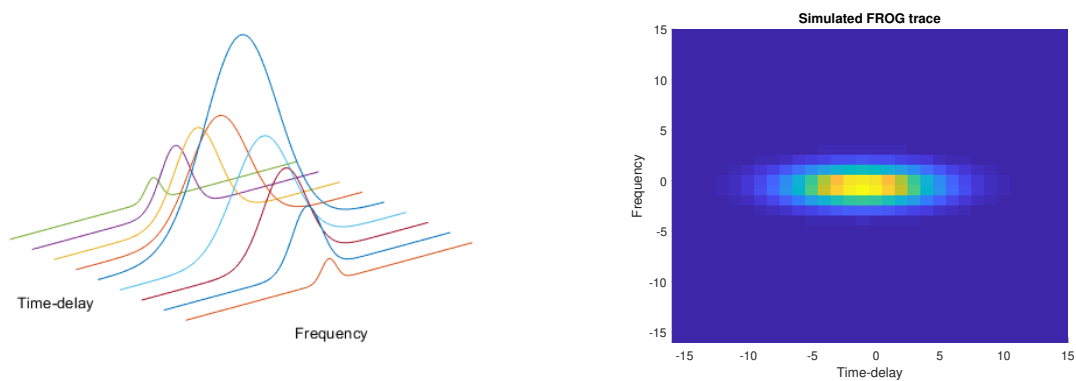


Figure 2.9: Visualisation and simulated sample spectrogram

Just as with the autocorrelator, the incoming signal is split using a beam-splitter, and then the signals are recombined in a nonlinear medium with a relative delay between the two introduced and one of many different nonlinear effects will take place. The signal measured by the spectrometer, the nonlinear electric field, is the Fourier-transform of the signal field and the gate field [5, chapter 5]

$$I_{FROG}(\omega, \tau) = \left| \int_{-\infty}^{\infty} E(t) g(t - \tau) e^{-i\omega t} dt \right|^2 \quad (2.23)$$

As with the case of the autocorrelator, the nonlinear electric field strength is proportional to the degree of which the signal field and the gate field are temporally overlapping as well as the incoming electric field strength. Which form the gate function $g(t)$ takes depends on which nonlinear process is utilised. Typically second or third order non-linearities are used, each offering different benefits and drawbacks [5].

Common non-linearities used in FROG include *polarisation gating* (PG-FROG), *self-diffraction* (SD-FROG), *third-harmonic generation* (THG-FROG) and *second-harmonic generation* (SHG-FROG) [32] and for X-FROG *sum-frequency-mixing* is preferably used.

In the case of PG-FROG, the beams are separated and recombined in a nonlinear medium with 45° change in polarisation compared to each other. The gate pulse induces a change in refractive index in the nonlinear medium which is a third order non-linearity. Nonlinear medium for this application might for example be a piece of fused silica. The result of this is that the medium acts as a wave plate and slightly rotates the polarisation of the signal pulse [5]. This process is known as cross-phase modulation [5]. In the case of PG-FROG with signal field $E(t)$, the gate field in eq. (2.23) takes the form $|E(t - \tau)|$. Advantages of PG-FROG is that there are no known ambiguities, and the trace is intuitive. Potential disadvantages are that high quality polarisers tend to be thicker, which introduces dispersion to the pulse which in turn might affect the results [32]. Another disadvantage is that $\chi^{(3)}$ -order non-linearities all require strong electric fields to generate a good third-order signal. fig. 2.10 shows a PG-FROG set-up.

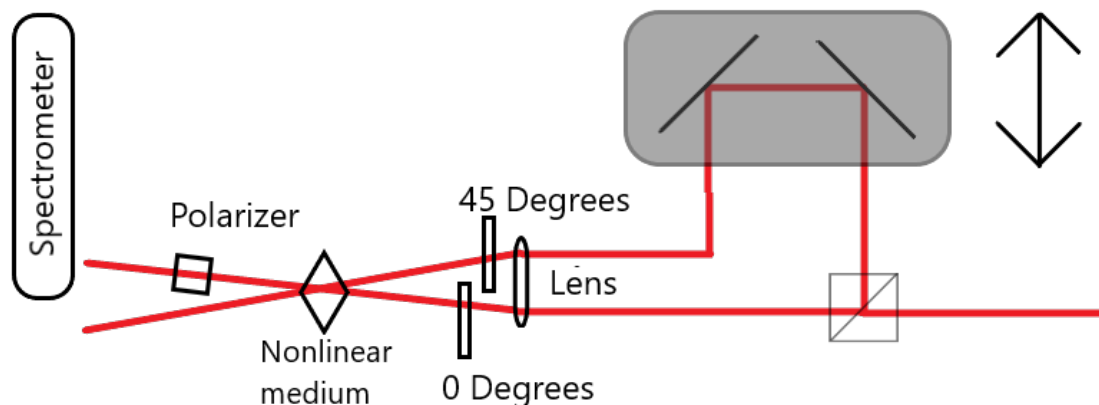


Figure 2.10: PG-FROG set-up

SD-FROG works in a similar fashion to that of PG-FROG, where a change in refractive index (Kerr effect) is utilised. Here, the two incoming beams into the nonlinear medium induces a grating in the medium which diffracts the beam. This beam can then be spectrally resolved to produce the SD-FROG trace [32]. This set-up is more sensitive to linear chirps as a chirp will change the induced grating and requires no polarisers to function[5]. The signals must recombine in the nonlinear medium with a small angle towards each other since the non-linearity here does not require phase-matching. In this set-up the gate-function takes the form $E(t)E^*(t-\tau)$ if the signal has the field $E(t)$ which gives the FROG-field $I_{FROG}(\omega) = \left| \int_{-\infty}^{\infty} E(t)^2 E^*(t-\tau) e^{-i\omega t} dt \right|$ which is measured according to fig. 2.11.

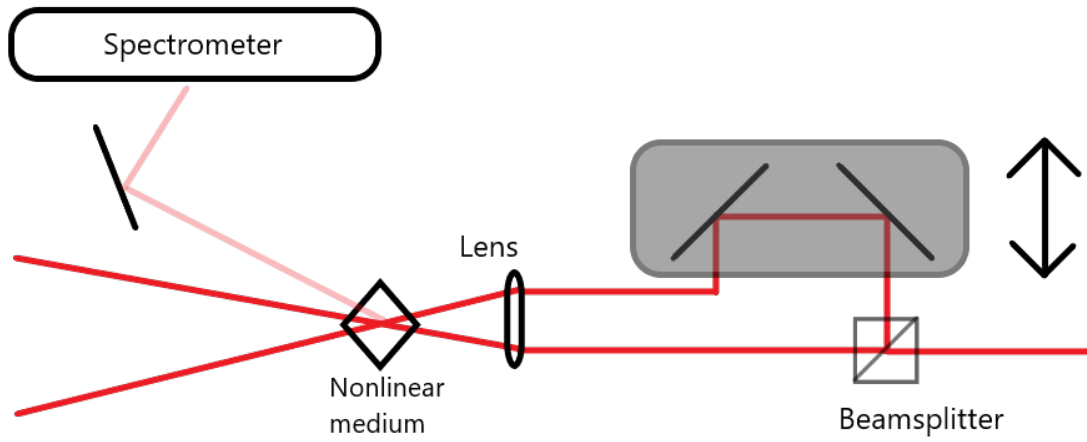


Figure 2.11: SD-FROG set-up

Another $\chi^{(3)}$ -FROG geometry is that of THG. In this set up, the nonlinear field takes the shape $E(t)^2 E(t-\tau)$ or $E(t) E(t-\tau)^2$ [33] depending on if the THG form the signal field or the gate field is measured. The geometry is similar to that of fig. 2.8 and the spectrometer is here placed along either one of the two arms. If this implementation of FROG is to be performed, caution needs to be taken. In this set-up a parasitic THG-mode may be present as the result of SFG between a SHG-mode and fundamental mode. These are often difficult to disentangle and as such it is hard to implement this geometry successfully without using a nonlinear medium which is centrosymmetric, which means that the medium shows *inversion symmetry*. Inversion symmetry means that the $\chi^{(2)}$ -susceptibility vanish and second order nonlinear effects will not occur, meaning that any THG mode is a true THG mode[21].

SHG-FROG is the most sensitive set-ups of FROG available, but has some disadvantages. In the case of SHG-FROG the incoming signal is split into two, then recombined after one has traversed a variable delay, to produce second harmonic generation. This is more sensitive compared to SD-FROG and PG-FROG due to SHG being a $\chi^{(2)}$ -process where as the other two uses a $\chi^{(3)}$ process meaning that weaker signals can be detected as second order non-linearities does not require as strong fields as third order non-linearities.. In the case of SHG-FROG the gate function is $E(t)$ which means that the full electric field measured by the spectrometer is

$$I_{FROG}(\omega, \tau) = \left| \int_{-\infty}^{-\infty} E(t) E(t - \tau) dt \right|^2 \quad (2.24)$$

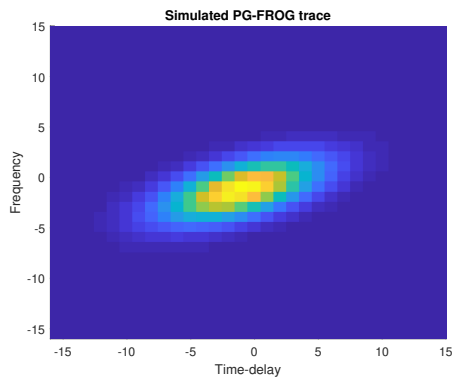
[34]. With SHG-FROG there is an ambiguity in the direction of time which means that the sign any chirp is ambiguous for this, more sensitive, implementation [5].

Furthermore, FROG may be implemented as *single-shot* or *multi-shot* device, where multi-shot refers to the measurement taking place over the span of several pulses whilst single-shot measures a single pulse. One implementation of a single-shot set-up is one referred to as GRENOUILLE [35] which stands for *Grating-Eliminated No-Nonsense Observation of Ultrafast Incident Laser-Light E-fields*. In this method, a Fresnel bi-prism is used instead to split the incident beam into two and then recombine them in a thick SHG-Crystal at a large angle relative to the normal of the crystal surface. One advantage with such a set-up is that split pulses are identical. In normal FROG an assumption that pulses are identical throughout the experiment has to be made as several pulses are used.

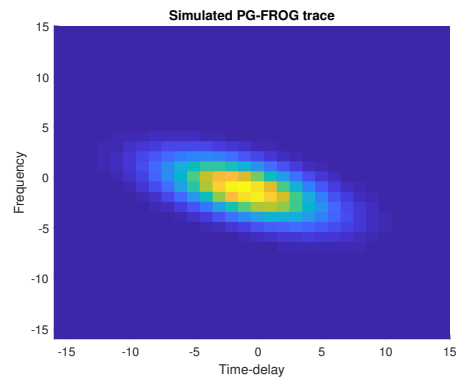
With these different implementations defined, the advantages and disadvantages of each may be summarised in table 2.1 and visualisations of different traces and effects of chirp can be seen in fig. 2.12.

Set-up	SHG	THG	PG	SD
Non-linearity	$\chi^{(2)}$	$\chi^{(3)}$	$\chi^{(3)}$	$\chi^{(3)}$
Sensitivity Single shot	0.01 μ J	0.03 μ J	1 μ J	10 μ J
Sensitivity Multi-shot	0.001nJ	3nJ	100nJ	1000nJ
Advantages	Very sensitive	Sensitive Large bandwidth	Intuitive traces automatic phase-matching	Intuitive traces
Disadvantages	Unintuitive traces	Unintuitive traces	Requirers polarisers	Requires thin- medium, not phase-matched
Ambiguities	Direction of time, relative phase of multiple pulses	Relative phase of multiple pulses	None known	None known

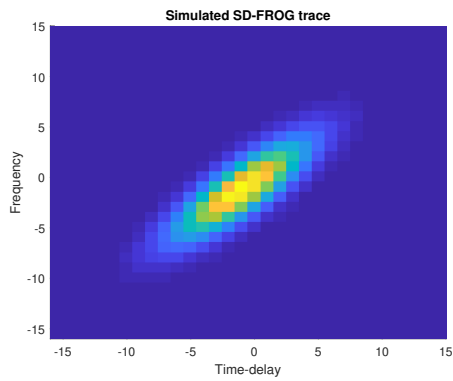
Table 2.1: Comparison of different FROG set-ups [32]



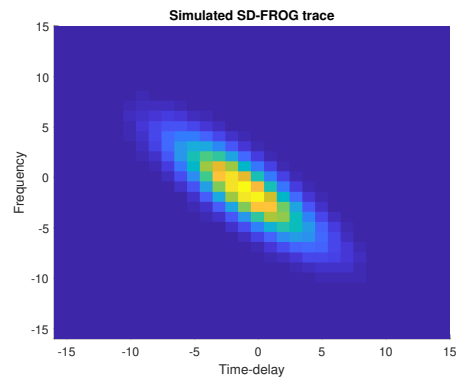
(a) Positively chirped pulse



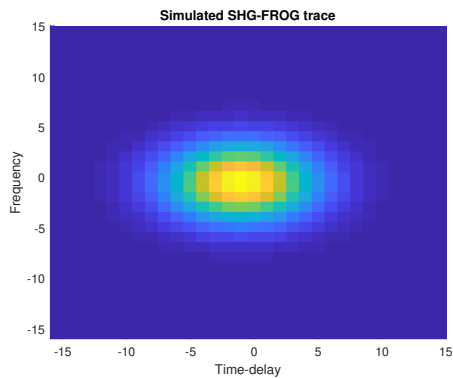
(b) Negatively chirped pulse



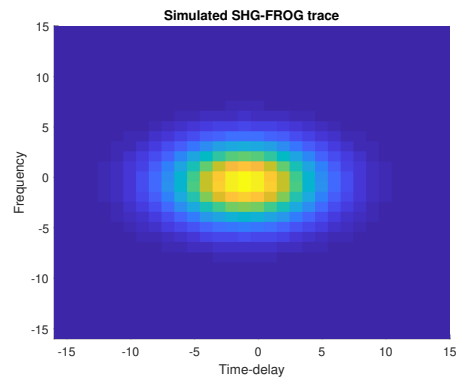
(c) Positively chirped pulse



(d) Negatively chirped pulse



(e) Positively chirped pulse



(f) Negatively chirped pulse

Figure 2.12: Simulated FROG-traces of positively and negatively chirped pulses. a) and b) shows traces for PG-FROG, c) and d) shows for SD-FROG and e) and f) shows for SHG-FROG

2.3.3 Cross-Correlation Frequency-Resolved Optical Gating

The purpose of this thesis however is to implement *cross-correlation frequency-resolved optical gating* (X-FROG) which is yet another altered version of FROG [6]. It works in very much the same way as the other implementations of FROG previously mentioned but here one of the arms recombined in the nonlinear medium is a previously characterised reference pulse. As a consequence of the relationship

in eq. (2.12) the higher order nonlinear polarisation field strengths are proportional to incoming field strength. This means that X-FROG can be used to characterise weak pulses as the reference can, in the case of a weak signal, be stronger to compensate for this [36]. Thus, with this in mind it is often preferable to use a $\chi^{(2)}$ -order non-linearity when doing an X-FROG measurement as $\chi^{(2)}$ -signals doesn't require as strong signal fields. fig. 2.13 shows a topological visualisation of SFG-XFROG which is the version that will be implemented for this thesis.

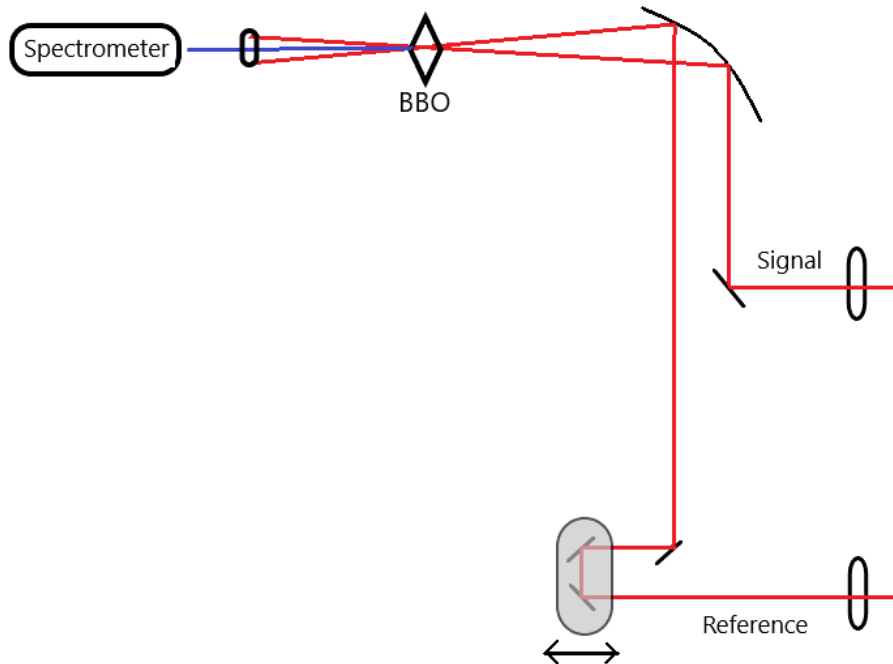


Figure 2.13: Cross-Correlation Frequency-Resolved Optical Gating. BBO stands for Beta Barium Borate which is the nonlinear medium chosen for this application

In the case of X-FROG, the reference is as previously mentioned an already characterised reference pulse, thus the FROG-intensity measured is the result of eq. (2.25)

$$I_{FROG}(\omega, \tau) = \left| \int_{-\infty}^{\infty} E(t) E_{ref}(t - \tau) e^{-i\omega t} dt \right|^2 \quad (2.25)$$

The spectrogram produced by this measurement is then analysed with the *frog algorithm* which extracts full amplitude and phase of the signal pulse.

2.4 Spider

SPIDER stands for *spectral phase interferometry for electric-field reconstruction* and is yet another method for characterising ultrafast laser pulses. In this set-up an incident field is split into three parts, two identical, temporally separated pulses

and one copy which is stretched in time with a dispersive medium [37, 10]. An interferogram is recorded between the time stretched pulse and the two replicas where the two replicas will produce interferograms with different frequencies due to them being mixed with the chirped, stretched copy.

This technique can provide the same information as FROG and has a much simpler extraction algorithm, but this is valid for a finite number of pulse characteristics. SPIDER requires the user to make a number of assumptions before extraction. One assumption needed is that the dispersion used to stretch one replica of the pulse is known. Another extraction is that the phase modulation is assumed to be the same for varying pulse intensities. FROG requires making no initial field assumptions and as such it is a more robust method. Further, algorithms today have a 100% convergence rating and have convergence times of a fraction of a second [38, 14, 13, 12]. For this reason, FROG as the option selected for implementation in the laser physics groups laboratory.

3

Method

The experiment performed for the purpose of this thesis is the implementation of a SHG-FROG as well as a SFG X-FROG. Thus, certain components needs to be selected for this purpose, most importantly the correct crystal.

3.1 Equipment

As is evident from fig. 2.13 the system consists of a number of different components. It is however, not a very complicated set-up and thus only a few pieces of key components needs to be acquired. Besides this, a commercial SHG-FROG is available with which verification of the set-up can be done. This commercial FROG will for the purpose of this thesis serve as a comparison and a tool for verification of the set-up which is to be constructed.

3.1.1 MesaPhotonics FROGscan

The commercial SHG-FROG available for use in the lab is one developed by MesaPhotonics called FROGscan [39]. fig. 3.1 shows a picture of the inside of the FROGscan and table 3.1 shows the parameters for this FROGscan.

Parameter	Value
Serial number	UF-1812-0155
Input pulse wavelength-range	450nm - >2000nm
Pulse-length range	15fs - 12ps
Temporal resolution	2fs or better
Delay-stage step-size	1fs
Real-time sensitivity ($I_{peak}I_{average}$)	4 W ²
Averaged sensitivity ($I_{peak}I_{average}$)	< 0.1 W ²

Table 3.1: Parameters for the commercial FROG

A beam line was set-up so that after a beam-splitter (to keep the same dispersion induced by the beam-splitter as the one measured in the constructed FROG/XFROG) the gate-signal could be redirected into the FROGscan.

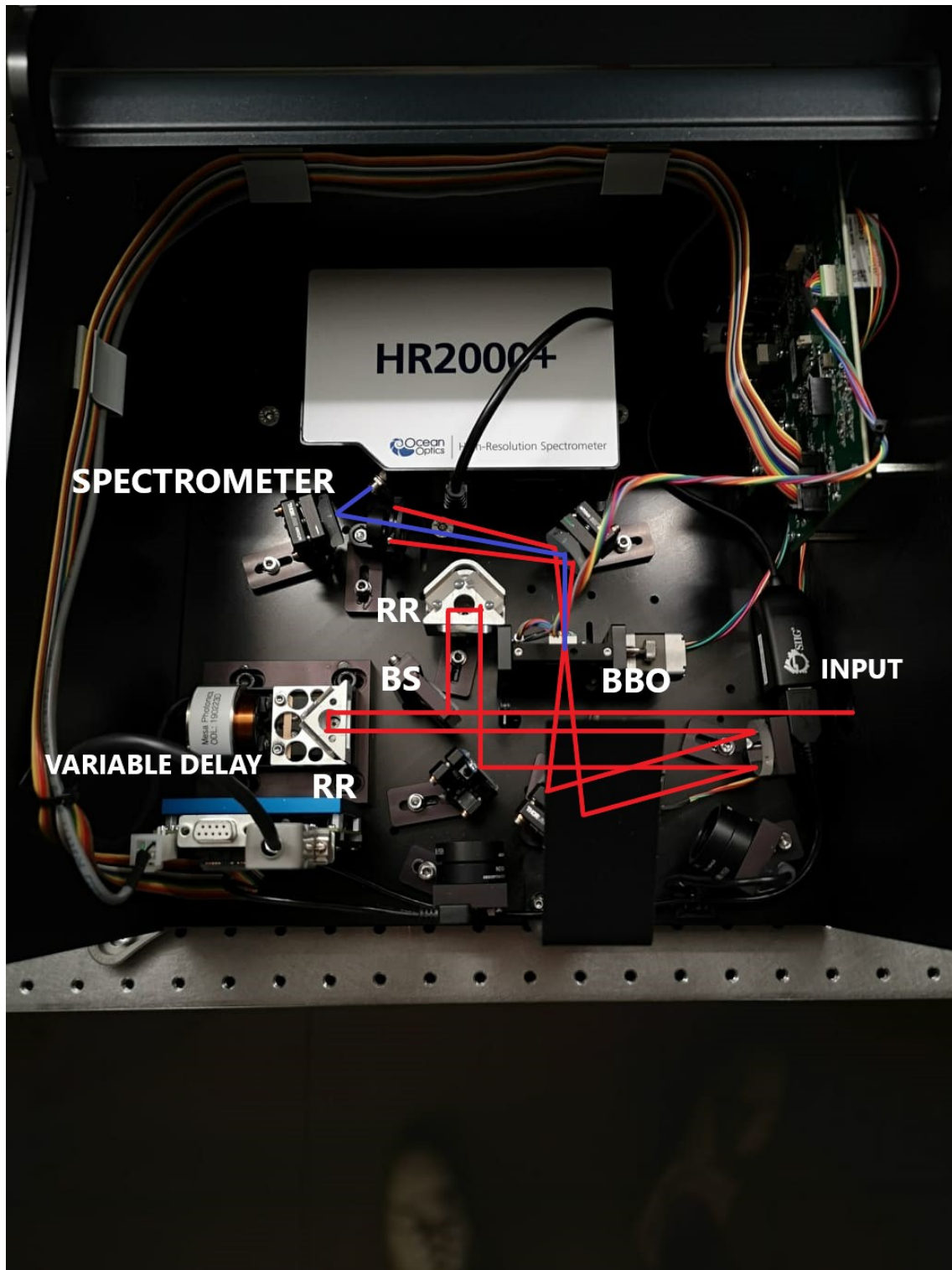


Figure 3.1: Inside of the FROGscan. Dark rectangle along the bottom is a platform upon which the top-cover rests. RR = Retro Reflector, BS = Beam Splitter

3.1.2 Laser

The laser which will act as the source of the ultrafast laser pulses is a Tsunami Ti:Sa-laser oscillating at 800nm from Spectra Physics [40]. The average output power of this laser is 900mW and the repetition rate is 80MHz. The pulses from this laser oscillator is, as will be measured in this thesis, around 200-270fs long. This laser oscillator is picture in fig. 3.2.



Figure 3.2: Spectra-physics Tsunami Ti:Sa-laser

3.1.3 Optical platform

One of the goals of this thesis was that the FROG/X-FROG should be small and portable, which puts a restraint on the platform upon which the set-up is constructed. For this purpose, an optical table from Thorlabs was selected, measuring 30×30 cm, which on the scale of a laboratory-sized optical table, is small. This size should with the simplicity of the set-up in mind be sufficient.

3.1.4 Delay-stage

The delay-stage is one of the key components of the system, providing the fundamental principle of FROG/X-FROG and also a measure for the resolution of the system. Since spectrometer measurements are taken at different time delays τ , the parameter which defines what is included in the FROG trace is the spectrometers resolution and the step-size of the delay-stage.

3. Method

If a laser pulse is considered with a hypothetical width of 230fs this pulse corresponds to a, with the relationship $L = \frac{T_0}{c}$, roughly 70 μm spatial duration. In the algorithm implemented for this thesis and that is described in section 3.3.2, the FROG-trace needs to be a $M \times M$ -matrix, usually a $2^n \times 2^n$ -matrix is used. If n is chosen so that the trace is a 128×128 -matrix the required step-resolution would need to be

$$\frac{70\mu\text{m}}{128} = 546.9\text{nm}$$

This however only contains the FWHM of the pulse and not the entire pulse, as such the step size needs to be increased so that the entire pulse is included into the FROG trace. Experimentally, a step-size of 1.2 μm proved to be sufficient to cover the pulses from the Tsunami laser. This corresponds to a time-delay resolution of $d\tau = 2\delta x/c = 8\text{fs}$.

The choice eventually fell on Thorlabs "MTS25-Z8 - 25" shown in fig. 3.3. This delay-stage can move 34304 'clicks' per millimetre, which gives a spatial resolution of 29nm which is well within the requirements. The full parameters of the delay-stage can be seen in table 3.2. This delay-stage offers a 25mm path difference which corresponds to a 50mm path extension since the optical path is double (two-way travel).

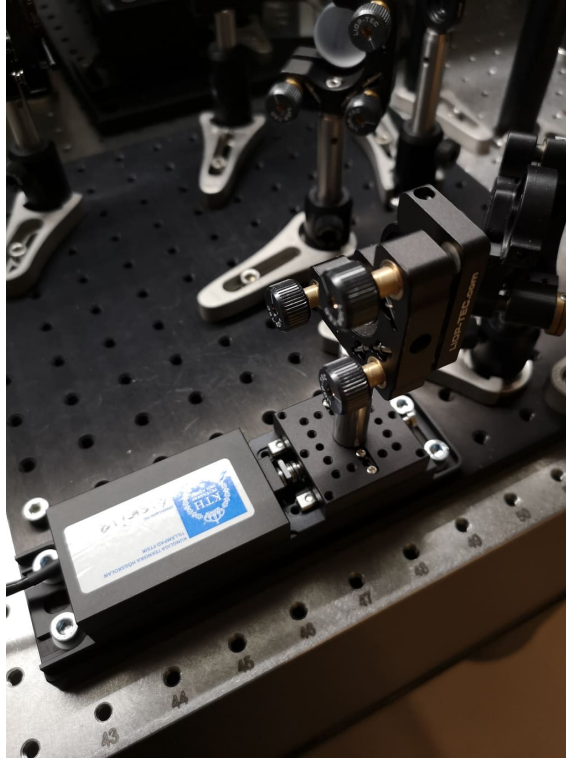


Figure 3.3: The MTS25-Z8 - 25 from Thorlabs.

This delay-stage won't work on its own however, it requires a 15-V voltage source and a controller to control it. Thorlabs recommends one of their own controllers for this delay-stage so it was chosen. The controller is Thorlabs KDC101 pictured in fig. 3.4.

Parameter	Value
Serial number	27504287
Translation range	25mm
Max velocity	2.4m s^{-1}
Minimum step-size	29nm

Table 3.2: Parameters for the MTS25-Z8 - 25 - delay-stage [41]

In the case of implementing a ptychographic algorithm, explained briefly in section 3.3.2, instead, the requirement for the FROG trace to be an $M \times M$ -matrix is removed [38].



Figure 3.4: KDC101 controller. Image from [41]

3.1.5 Parabolic mirrors

In order to generate sufficient intensity in the nonlinear crystal for SHG to occur the two beams needs to be focused onto the surface of the crystal. In order to achieve this parabolic mirrors with a focal length of 10.1cm and 15.0cm will be used.

3.1.6 Nonlinear crystal

The most important part of the set up is the nonlinear crystal used to produce SHG. A suitable crystal which provides a good $\chi^{(2)}$ -susceptibility, and that is thin enough to cover the bandwidth of the laser needs to be chosen.

The choice fell on a Beta Barium Borate (BBO) crystal. This crystal is optically transparent over the wavelengths it will be subjected to for this thesis and it has a strong second order nonlinear susceptibility. Furthermore, the crystal is ordered

to be 100 μm thin so that broadband pulses can be used with it. This thickness combined with the laser above at 800nm gives a phase-matching bandwidth of $\Delta\lambda = 31.96\text{nm}$ with the use of eq. (2.18). This is well above the roughly 8nm signal provided by the Tsunami laser.

Since broadband research is conducted at the department of Laser Physics at KTH, a crystal with a sufficiently large phase-matching bandwidth is required. The previously discussed trade-off between phase-matching bandwidth and conversion efficiency needs to be revisited to select an appropriate crystal. Since the bandwidth is a constraint on the system, the width is initially selected to accommodate this. For this reason a 10 μm BBO-crystal has been acquired which, again with eq. (2.18), yields a phase-matching bandwidth if $\Delta\lambda = 267.8\text{nm}$ for a 800nm signal. The conversion efficiency will reduce due to this. In this situation however, the thin crystal needed for the phase-matching does not mean that a compromise on conversion efficiency is done, but rather that a constraint on sensitivity is introduced. This is remedied somewhat by creating an X-FROG set-up, where the reference may compensate somewhat for this reduction in conversion efficiency by having enough power to still yield the second order mode.

3.1.7 Spectrometer

The last component that needs to be acquired is a spectrometer with which to measure and construct the FROG trace. In the conventional algorithm implemented in this thesis, where the traces are $M \times M$ -matrices, the maximum resolution is predetermined by the grid-size as $\delta\tau\delta\omega = 1/M$ where $\delta\tau$ is the time-step in the delay-stage and $\delta\omega$ is the frequency resolution of the spectrometer [42] [43]. With the above $d\tau = 8\text{fs}$ and a grid-size of $M = 128$, the spectral resolution required is 0.5212nm for a 400nm SHG-signal.

The choice fell on Avantes' "AvaSpec-Mini2048CL-UVI25" spectrometer in fig. 3.5 [44]. It covers wavelengths from 200nm to 1100nm with 2048 pixels and the electronics are integrated into the device. This pixel count and wavelength range provides a resolution of 0.4395nm. It communicates and powers with a USB-cable which is a simple straightforward approach to implement. Some parameters for the spectrometer is available in table 3.3

Parameter	Value
Serial number	1811088M1
Pixel count	2048
Wavelength-range	200-1100nm
Resolution	0.4395 nm
Sensitivity	337500

Table 3.3: Parameters for the AvaSpec-Mini2048CL-UVI25 spectrometer [45]. Sensitivity given in counts per μW per seconds integration time.



Figure 3.5: Spectrometer used

3.2 Construction

Construction of the set-up is a fairly straight-forward process, some minor choices needs to be made however in order to maximise space efficiency.

One part that can not be compromised with is the delay-stage which is the biggest component spatially so this will simply be installed in a corner and then the rest of the set up will have to be worked with from this. The idea is to mount a retro-reflector on top of the delay-stage and this will then be used as the variable delay for the experiment.

With the case of FROG, only one incident pulse exists so thus the beam-splitter

would be placed inside the set-up. In this case however, the purpose is to build an X-FROG, in which the number of incident pulses are two. Thus, two input apertures will be installed along the edge of the optical platform. These will serve as inlets for the pulses, and the optics inside will guide them to their destination. Since as previously mentioned, one laser will be used to test and verify the set-up, a beam-splitter will be placed outside of the set-up which will create the signal and the reference pulse. This will also allow the signal to be modified, examples are passing the signal through dispersive mediums or passing it through a pulse compressor.

One condition for successful FROG/XFROG-measurements is that the incident fields have the same pulse repetition rate so that a parasitic delay is not introduced for each pulse. This is easily solved by using the same laser as signal and gate, which is also most often the case of how X-FROG is performed.

Initially the idea was to use two available parabolic mirrors to focus the two beams into the crystal, but this proved to be troublesome. The two available parabolic mirrors had different focal lengths, and spatially overlapping them in the focus, while also meeting the phase-matching condition proved to be difficult. On top of this, in the confined set-up of 30×30 cm the 15.0cm-focal-length mirror proved to be difficult to work with while not letting it occupy too much space.

To overcome this, the two pulses were changed so that the two pulses are now incident parallel against each other on one of the parabolic mirrors, and thus they will automatically spatially overlap in the focal point, and only the parabolic mirrors vertical reflection angle needs to be optimised to achieve proper phase-patching. After the components are placed and the set-up is aligned, it only remains to slide in the crystal and rotate it and to move the delay-stage around until the beams arrive perpendicular to the surface of the crystal whilst temporally overlapping and SHG can be observed. The resulting set-up is pictured in fig. 3.6.

The resulting SHG mode can then be measured with the previously mentioned spectrometer. The SHG mode has been coupled both via a fiber and through free space coupling.

3.3 Software

The X-FROG set-up has two piece of softwares that it needs to run. The first software that needs to be created is a control interface to control both the delay-stage and the spectrometer. These needs to be synchronised and work together to create the different delays, measure different spectrums, and to output the measured data in a suitable file format.

The second software that needs to be written is the muscle of the X-FROG set-up, the algorithm that from the spectrogram extracts the gated pulse. A lot of theory has gone into refining the algorithm and the history and development of the algorithm will be explained in detail.

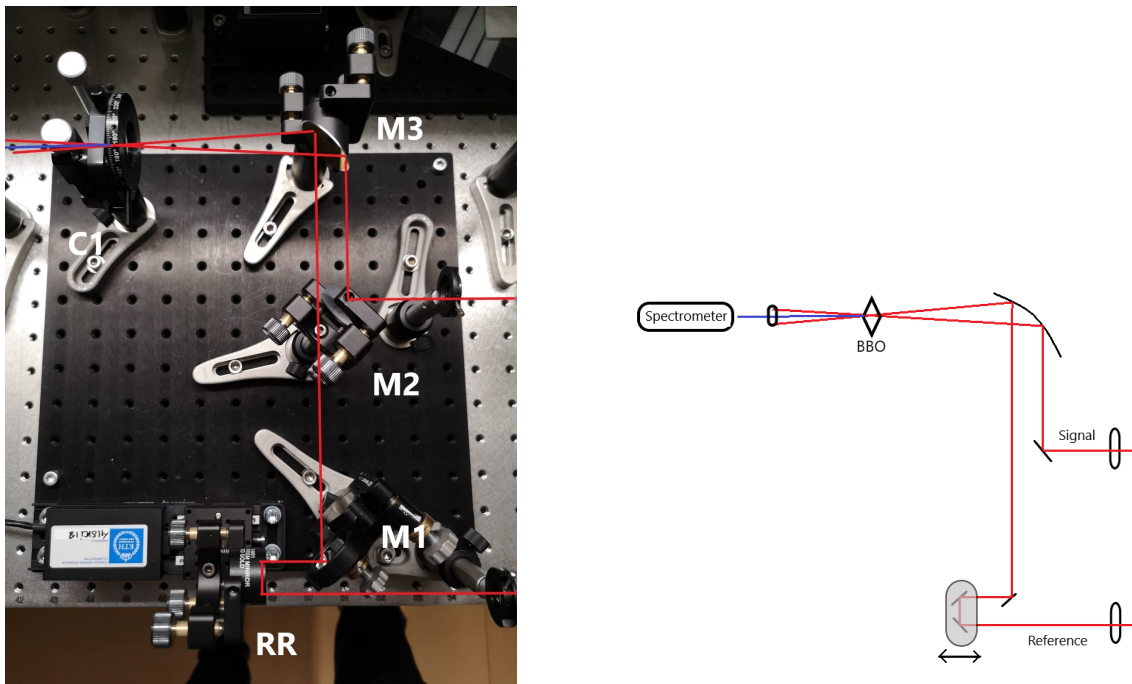


Figure 3.6: Picture and topological sketch of final set-up

3.3.1 LabVIEW

Both the spectrometer and the delay-stage needs to be controlled through a piece of software so that they work together and in a controlled manner. They both have individual softwares to control them, but they work independently from one another. It is possible to control them one by one and manually construct a FROG-trace but this is tedious and will take more time than necessary, and as such a new software needs to be created so this process can be automated.

Both pieces of hardware comes with libraries suitable for use in a programming environment called LabVIEW [46]. LabVIEW is a graphical programming tool where programming is done in a "flowchart-manner". A flowchart of the LabVIEW programs functionality is found in fig. 3.7 and screen-shots of actual LabVIEW-environment in fig. A.1 and fig. A.2 in the appendix. The resulting LabVIEW program interface is shown in fig. 3.8.

When the software is executed the spectrometer and the delay-stage needs to both be plugged in for it to not throw an error towards the user. The user then initialises the program, during which the connection to the spectrometer and delay-stage is created and the settings for both are set-up. After this is done, the user can do a number of things. To the left is a column which has all the different settings and parameters for the spectrometer. The user can change these settings to alter things as smoothing parameters for example, but four out of the first five are those that are of most importance to the functionality of the FROG.

These parameters are start- and stop-pixel which to include in the measurement, integration time and number of averages to perform. The start- and stop-pixel

3. Method

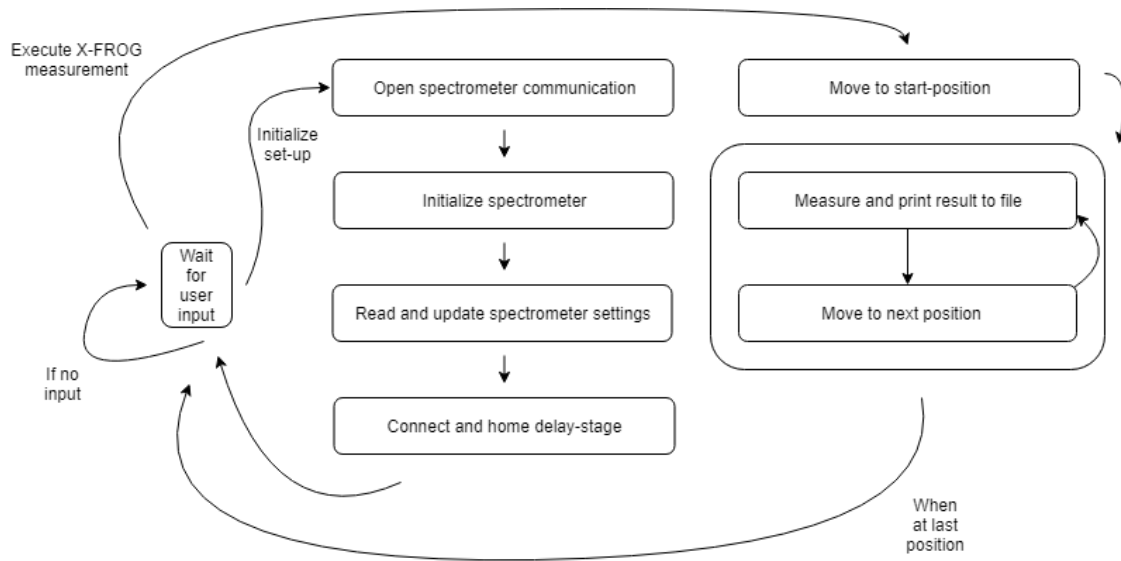


Figure 3.7: Flowchart of the LabVIEW programs functionality

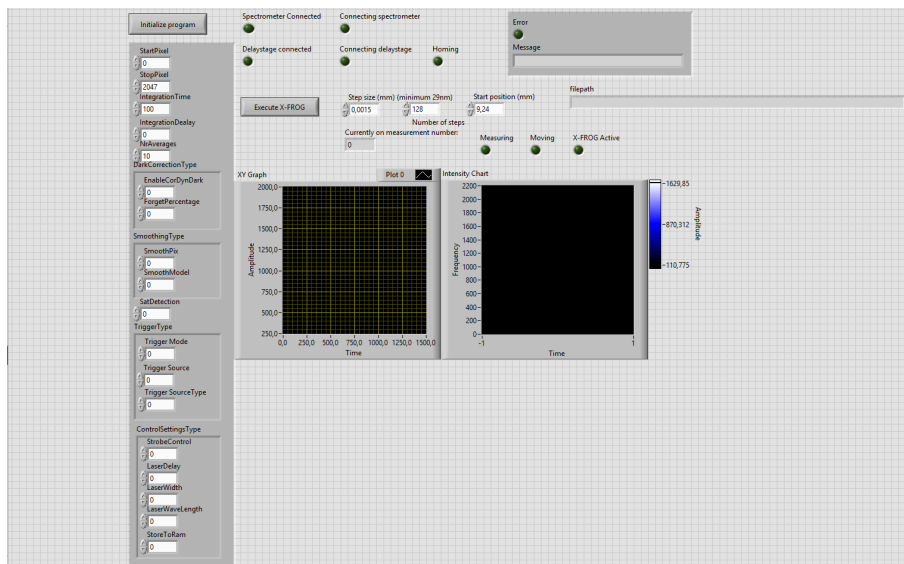


Figure 3.8: LabVIEW-interface of the frog-software

parameters determine how many and which pixels that will be included in the next measurement. This may be centered around the wavelength required and then reduced to the dimensions needed. The resolution will not improve but the size of the result file will be decreased. The integration time is for how long the detector will be measuring. Here there is an obvious relationship between the value and the time a FROG-measurement takes. The number of averages determines how many consecutive measurements the spectrometer will take and average over. An increased number of averages should average out the noise and thus lower the noise floor. Experimental results however determined that after about 10 averages no further reduction in noise floor level was detected and this is thus a suitable setting.

If no errors were detected during initialisation, the user is free to perform a FROG-

measurement. The delay-stage has a 25mm range, and the user needs to find 'where' on this variable delay the temporal overlap occurs. This can be done before program execution by using a joystick on the controller. The user provides the program with the location at which temporal overlap begins, then enter the desired grid-size and lastly the step size of the delay-stage. When all these parameters are set-up, and the final position does not exceed 25mm, the program starts the experiment. If the settings take the final position of the delay-stage beyond 25mm, the delay-stage controller will throw an error to the user.

It runs the delay-stage to the entered start position after which the first measurement is made. The delay-stage waits for the spectrometer to measure and let LabVIEW know the results, before it moves again after which a new measurement is made and so forth until all of the measurements are done. During this time, after each measurements, results are continuously written to an output file, where vectors containing the spectrometers wavelength-values, spectrometers measured values and the position of the delay stage is logged.

The resulting file is named according to "results-date-time.txt" and these files are then fed to a Matlab software which creates a spectrogram out of the methods and then performs the extraction algorithm.

3.3.2 Matlab

As have been previously mentioned, the key component to FROG and X-FROG is the FROG-algorithm which takes a FROG/X-FROG trace as input and extracts amplitude and phase of the signal field.

The simplest and shortest explanation of the FROG-algorithm is that it is an algorithm that takes a FROG-trace and attempts to guess the signal field that produced the trace. After a guess has been made, the algorithm evaluates how good of a guess this is, and is either happy with the result or starts over and generates a new guess based on the previous guess. A visualisation of the iterative process is shown in fig. 3.9

In this thesis the experimental set-up has resulted in a SHG-FROG and a SFG-XFROG set-up. This means that, as have been mentioned before, the nonlinear field for the case of SHG-FROG is [28]

$$E_{sig}(t, \tau) = E(t) E(t - \tau) \quad (3.1)$$

and for SFG-XFROG it is [47]

$$E_{sig}(t, \tau) = E(t) E_{ref}(t - \tau) \quad (3.2)$$

where E_{ref} is an already characterised reference pulse. The algorithm involved in extracting the incident fields are called *principal components generalised projections algorithm* (PCGPA).

During the initial execution of the algorithm it is fed a FROG-trace as well as an initial guess for the incident signal field, and in the case of SFG-XFROG it is also

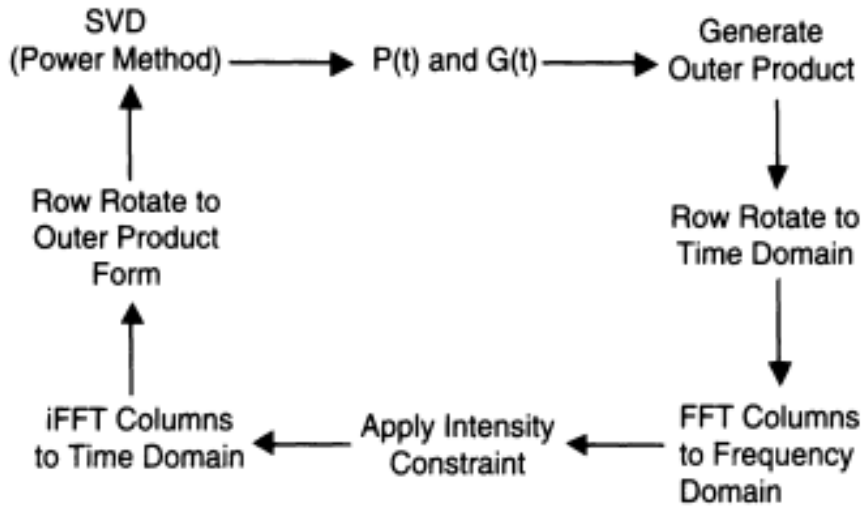


Figure 3.9: Iterative process, image from [5]

fed the previously characterised reference field. If the incident signal field is referred to as $E(t)$ and the gate field $G(t)$ where the gate field is either a time-delayed copy of the signal field or the reference field in the case of X-FROG, an outer product matrix can be created by multiplying them with each other [5, chapter 21].

$$\mathbf{O} = \begin{bmatrix} E(t_1)G(t_1) & E(t_1)G(t_2) & \dots & E(t_1)G(t_n) \\ E(t_2)G(t_1) & E(t_2)G(t_2) & \dots & E(t_2)G(t_n) \\ \vdots & \vdots & \ddots & \vdots \\ E(t_n)G(t_1) & E(t_n)G(t_2) & \dots & E(t_n)G(t_n) \end{bmatrix}$$

This matrix can be converted into a time-domain FROG trace by circularly rotating the n -th row $n - 1$ positions.

$$\hat{\mathbf{O}} = \begin{bmatrix} E(t_1)G(t_1) & E(t_1)G(t_2) & \dots & E(t_1)G(t_n) \\ E(t_2)G(t_2) & E(t_2)G(t_3) & \dots & E(t_2)G(t_1) \\ \vdots & \vdots & \ddots & \vdots \\ E(t_n)G(t_n) & E(t_n)G(t_1) & \dots & E(t_n)G(t_{n-1}) \end{bmatrix}$$

Here the first column of this new matrix $\hat{\mathbf{O}}$ represents the nonlinear field where the time delay between the signal and the gate is $\tau = 0$, the second column represents the $\tau = -\Delta t$ and so forth. By rearranging the columns so that the column representing $\tau = 0$ is in the center of the matrix and then Fourier transforming the columns, the frequency-domain FROG trace has been created. The steps of this method is shown in fig. 3.10. To summarize it, the outer product is created, the rows are shifted to simulate the time delay between the signal and the gate, then it is re-centered around the middle after which the columns are fourier transformed to create the frequency-domain FROG trace.

At this point, the algorithm applies one of two constraints, and that is that the

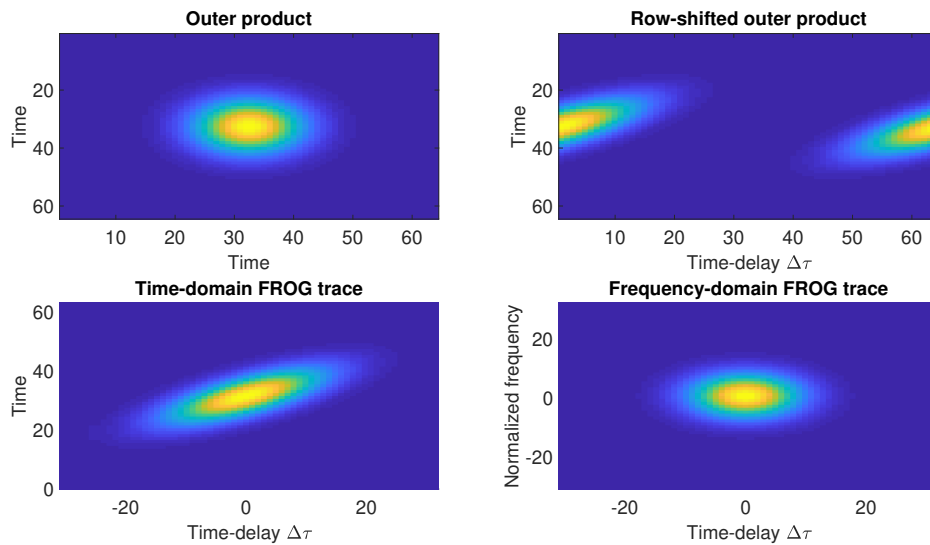


Figure 3.10: Construction of simulated FROG trace. Arbitrary units

intensity of the simulated trace is replaced with that of the measured trace

$$E_{replaced}(\omega, \tau) = \frac{E_{simulated}(\omega, \tau)}{|E_{simulated}(\omega, \tau)|} \sqrt{I_{FROG}(\omega, \tau)} \quad (3.3)$$

This means that the intensity will be the same but the phase of the simulated FROG trace will be kept.

The second constraint the algorithm works with is that the next guess for the incident field must minimise the frog error G

$$G = \sqrt{\frac{1}{N^2} \sum_{\omega, \tau=1}^N (I_{FROG}(\omega, \tau) - |E_{sig}(\omega, \tau)|^2)^2} \quad (3.4)$$

where N is the dimension of the FROG trace.

The above mentioned process to simulate a FROG trace is then reversed with this new FROG trace with its intensity replaced and it arrives at a new outer product matrix. The goal of minimising the error function with the next guess is automatically fulfilled if the method of *singular value decomposition* (SVD) is applied. SVD takes a matrix and calculates three matrices U , S and V , where the rows of U and the columns of V respectively are the eigen-vectors for the signal and gate field vectors which would produce the outer product matrix, with the values in the diagonal matrix S being the relative weights of each eigen-vector [48].

Yet another method for reducing the error function and that is computationally more efficient is the *power method*, which reduces the SVD step into a simple matrix multiplication [5] [49]. Given the outer product matrix O and the previous guess P^i the next guess can be estimated via

$$P^{i+1} = OO^T P^i \quad (3.5)$$

If the set-up would have been one that is not SHG-FROG, the gate field G can be solved for in a similar fashion

$$G^{i+1} = \mathbf{O}^T \mathbf{O} G^i \quad (3.6)$$

Since in SHG-FROG the gate and signal is the same, $P = G$.

This algorithm can with some minor modifications be used for extraction of signal field from SFG-XFROG traces as well. In this scenario, one more constraint is available since the gate field is already known and kept the same for each iteration. The result of this is that only one set of eigen-vectors needs to be solved for, and thus computation time decreases. Convergence also typically occurs in fewer iterations [5].

There is another algorithm available referred to as *time-domain ptychography* which has a different approach than that of the above described FROG algorithm. This method involves different methods for generating new guesses for the signal and gate, and the benefits of this method is that the sampling constraint $\delta t \delta \omega = \frac{1}{M}$ is removed. Furthermore, this algorithm does not require as many temporal delay-steps and as such the number of data-points can be reduced and the convergence time improved [38, 14, 13]. This algorithm has not been implemented however due to time constraints involved in the nature of a master thesis project. The PCGPA was preferred as the similarity between SHG-FROG and SFG-XFROG pulse-extraction meant time-efficient implementation and for quick reference pulse characterisation for X-FROG measurements.

4

Results

4.1 SHG-FROG

During construction of the set-up, it was noticed that the 100 μm thick BBO-crystal had cracked during the process and needed replacing. A 200 μm thick alternative BBO-crystal was found in the lab which replaced the original after which work could continue as planned. The thickness of the new crystal provides a narrower bandwidth over which the FROG/X-FROG will be functioning at roughly 16nm according to eq. (2.18) but this is still well within what is needed for testing of this set-up with the Tsunami laser. In the future for characterisation of broadband pulses, this needs to be replaced with a thinner crystal.

First measurements were made which would verify if the FROG-algorithm implemented would be working as intended. The results of these measurements will then be compared to the results provided by the commercial FROG to make sure that it is working properly. Several measurements were made, during which the LabVIEW software proved to be working as intended. Several measurements were made for varying grid-sizes. Due to the software being easier to implement with $M \times M$ -matrices, the number of steps in the delay-axis also decided the number of pixels to include in the frequency-axis. The whole pulse spectrum was included however for 32×32 , 64×64 , 128×128 and 256×256 so no information was ever lost but the benefit of using smaller grid sizes were aesthetic only apart from the software running faster.

The results for both the commercial FROG and the constructed FROG was consistent over several measurements with regards to temporal width except for them both showing a small variation. This is possibly and most likely due to an unstable laser. fig. 4.1 shows a measured and reconstructed SHG-FROG trace and fig. 4.2 shows the difference between the measured and reconstructed trace. The results for the SHG-FROG can be found in table 4.1 along with the averaged result of ten measurements with the commercial FROG. Measurements showed that SHG has, as predicted, an ambiguity in the sign of the pulse chirp. This ambiguity can be corrected for by redoing measurements with a piece of glass inserted into the laser beam. Chromatic dispersion will tell us if the pulse is up- or down-chirped if the initial change in pulse width is negative or positive. Experiments were performed with a piece of BK7 glass with a dispersion parameter such that shorter wavelengths travel at slower speeds than longer. This means that if the pulse is up-chirped, the pulse will broaden and if

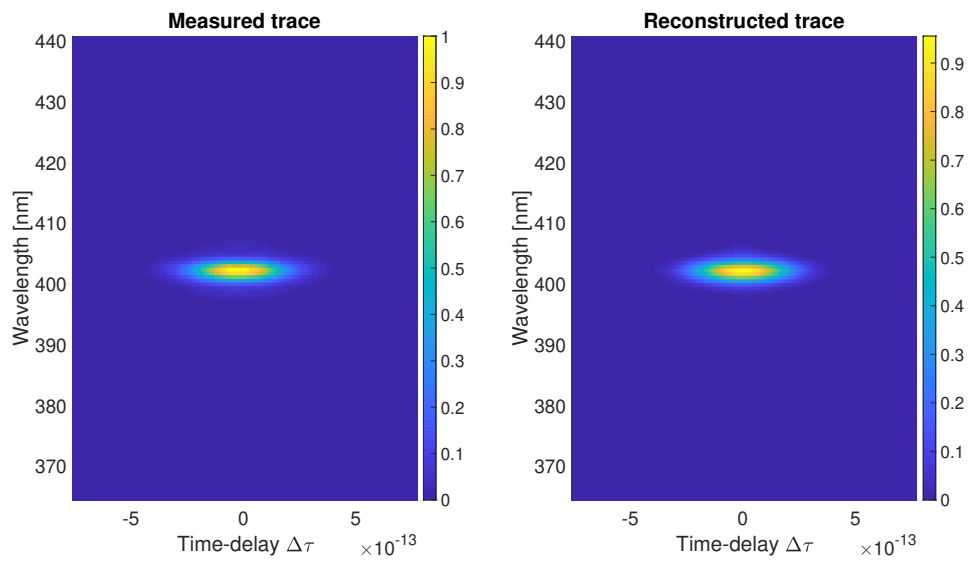


Figure 4.1: Normalised measured and reconstructed trace from the constructed set-up

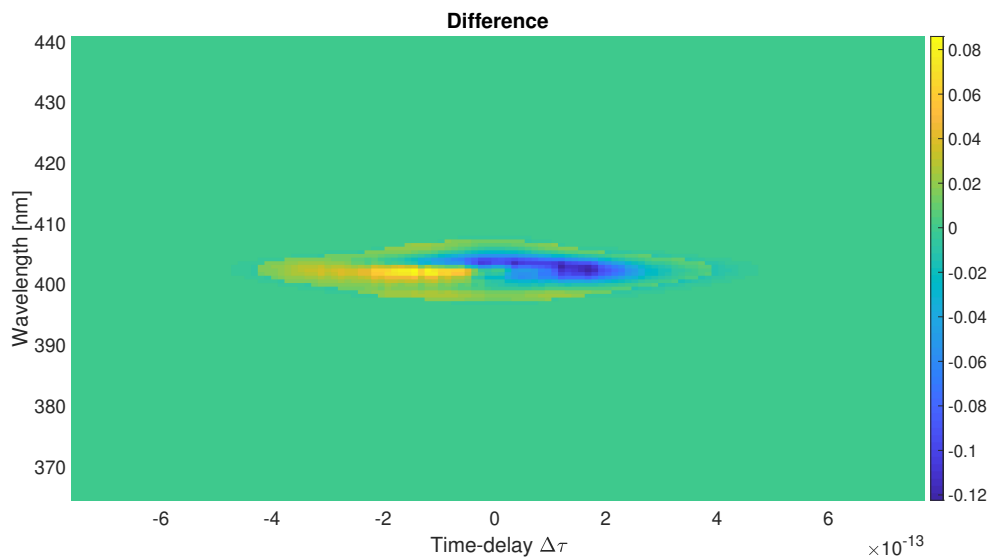


Figure 4.2: Difference between measured and reconstructed trace. Reconstructed phase correspond to a FROG error $G = 0.006$

the pulse is down-chirped it will compress. Experiments with both the constructed set-up and the commercial FROG showed that an initial broadening occurred and as such the pulse is up-chirped. This means that the problem of direction-of-time ambiguity is removed by performing this extra experiment.

SHG-FROG Measurement #	FWHM (fs)	Chirp	Bandwidth (THz)	TBP
Average	$254.4^{+12.6}_{-13.4}$	$0.3957^{+0.1802}_{-0.1424}$	$1.95^{+0.03}_{-0.06}$	$0.4706^{+0.0055}_{-0.0165}$
Commercial Average	$241.7^{+9.44}_{-6.32}$	1.8	3.77	0.91

Table 4.1: Results from 5 consecutive FROG measurements

Interesting to note here in the results from the FROG measurements are that the retrieved pulse temporal width from the constructed set-up corresponds well with the results from commercial FROG. The remaining values however differ by roughly a factor of 2.

The difference in bandwidth and TBP comes from the fact that the retrieved phase differ from what the commercial FROG retrieves, and this difference in phase is what needs to be looked more at. Over the width of the pulse the phases appears to show, according to fig. 4.3, second order polynomial phases. A linear chirp. The phase fluctuates between measurements and as such this might indicate an error with the measurements. Further, fig. 4.3 shows a clear trend in pulse shape and this corresponds well to pulse shapes retrieved by the commercial FROG. fig. 4.4 shows an averaged pulse as well as a Gaussian fit.

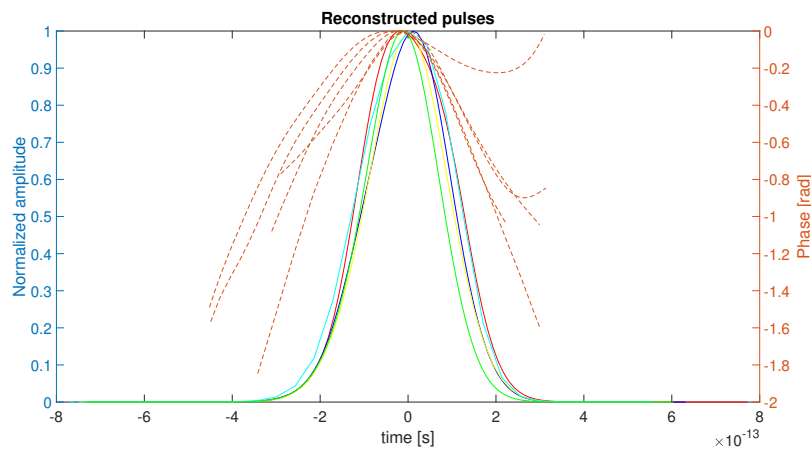


Figure 4.3: Reconstructed pulses from SHG-FROG measurements

Reasons however for the bandwidth and chirp being a factor two wrong is yet undetermined. If the algorithm is provided a simulated trace it solves completely for the electric field in both the case of SHG-FROG and SFG-XFROG. If the algorithm is provided with spectrograms from the commercial FROG, it produces an extracted pulse similar to that which the commercial FROG gives. A full comparison here between the pulse retrieved by the commercial FROG and that which the implemented Matlab algorithm extracts with the commercial FROGs traces is not possible however as the commercial FROG does not provide a lot of information besides pulse parameters (such as axis values) and only an estimation can be done. The conclusion drawn from this is that it appears that the algorithm is doing what it is supposed to do and that the error is somewhere else to be found. In the next

4. Results

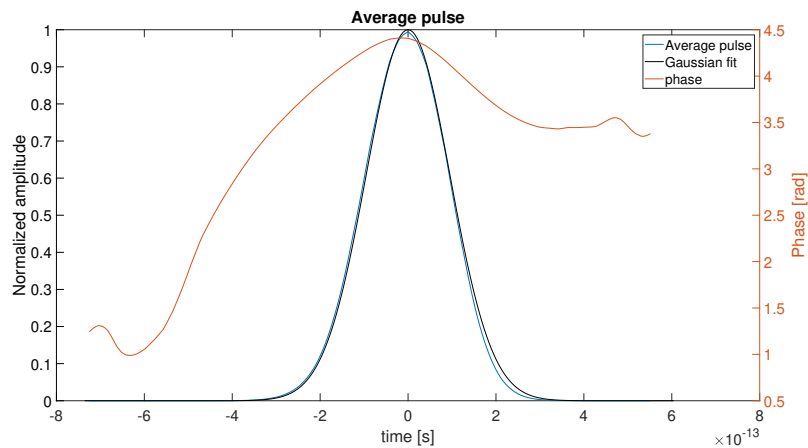


Figure 4.4: Average pulse with phase and gaussian fit

section retrieval of simulated X-FROG traces show that the algorithm should work as intended.

By examining the trace visually, nothing appears to be wrong as it is symmetrical and is centered around the correct wavelength. However when one examines the spectrum corresponding to $\tau = 0$ it appears that the problem may come from the measurements themselves. Both inspected trace and spectrum is here shown in fig. 4.5. If this is compared to fig. 4.6, which is a reference spectrum output by the oscillator which the oscillator is tuned towards, it is obvious that there are some differences. fig. 4.6 is a reference spectrum of the fundamental mode and fig. 4.5 shows that of the SHG mode which is the reason for the different center wavelengths. Interesting to see here is that the spectrum seem to have lost its profile, even though the BBO should have phase-matching bandwidth well above what is required.

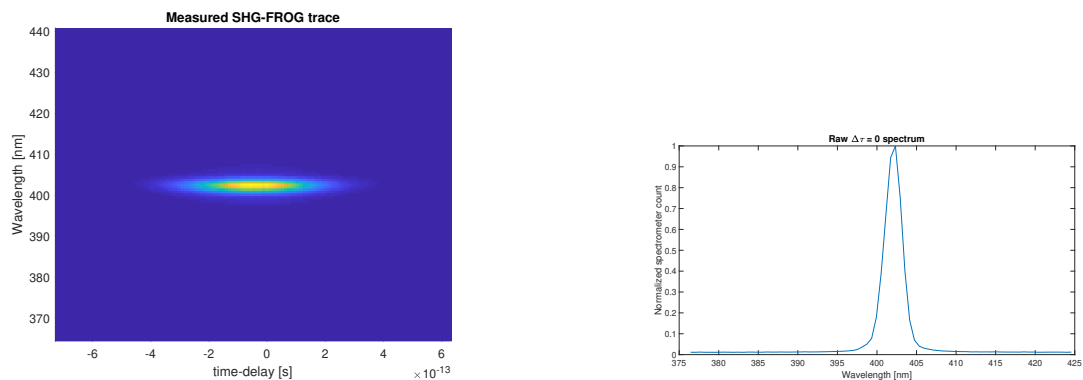


Figure 4.5: Measured SHG-FROG trace and raw spectrum

The cause for this abnormal spectrum has not yet been determined. Possible reasons include the coupling of the SHG into the spectrometer. Coupling of the SHG-mode into the spectrometer was done with both a fiber and via free-space coupling. It could be that the fiber itself has degraded in quality or that the spectrometer was not correctly aligned when free-space coupled. One other possibility is that the spectrometer is not working correctly, but this needs verification. One last possible

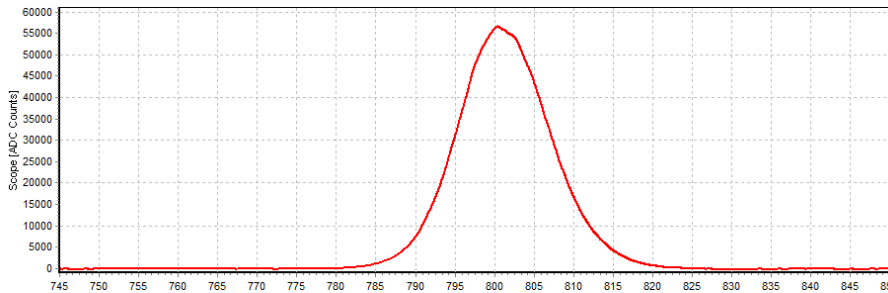


Figure 4.6: Fundamental harmonic spectrum

source of error is that the 200 μm BBO-crystal used have defects not visible by the naked eye which prohibits successful SHG. In the future further experiments need to be done with the 10 μm BBO-crystal to see if the defects are still present.

4.2 X-FROG

The final purpose of the thesis work was to construct a set-up capable of performing X-FROG measurements as research at the laser physics group involves, among other things, generation of broadband pulses. As such, it is beneficial to know the pulse both before and after the experiment, which is the reason X-FROG is suitable. Previous results from the SHG-FROG measurements show that there is an error present in the measured spectrums and as such the results regarding chirp, bandwidth and phase can not be trusted. It appears however that the temporal width of the pulses are possible to obtain as the retrieved temporal widths correlate well with that of the commercial FROG which appears to be working as intended. This would seem to be the case since the detection is made over the central frequencies of the pulse and that it is further away from the central wavelength that the detection is erroneous. Thus, the X-FROG 'blob' in the spectrogram has the correct x-axis components and incorrect y-axis components. In essence, the algorithm with such spectrograms acts like an autocorrelator where no assumptions need to be made, and the temporal width is retrieved correctly without distortions.

With this said, X-FROG measurements can still be performed with a signal that is different in time rather than in frequency. As such, the previously used piece of BK7 used to determine the chirp direction by inserting it into the beam path at the oscillator, can now be inserted into the signal path of the SFG-XFROG instead, thus providing one beam which is the previously characterised reference, and the other being the altered signal that is unequal to the reference. Since the constructed SHG-FROG measurements show an error, retrieved pulses from the commercial FROG is instead used as the reference in Matlab. This pulse should be the same as the actual one into the constructed SFG-XFROG as the commercial frog should introduce no alterations to the pulse.

The piece of BK7 used previously has a thickness of 10mm and with eq. (2.9) the change in width is estimated to be 10fs with a dispersion coefficient of $D =$

4. Results

$-131.42\text{ps nm}^{-1} \text{ km}^{-1}$. These measurements together with the retrieved pulses from the commercial FROG as the reference proved to be inadequate to work with. The FROG error G is too big at around 20% - 25%. These error values indicate that the results provided can not be regarded as correct when the commercial FROGs pulse is used as a reference until the erroneous measurements are fixed, after which it should be possible.

If instead the pulses retrieved by the SHG-FROG constructed is used, the same error in spectrum is present in both gate and signal, and as such temporal width retrieval should still be possible. These experiments proved more successful with errors once again down at 0.X%. table 4.2 shows the results from these measurements. Over these measurements the broadening showed to be 13.5fs which is close to what the theoretical value was estimated to be and within what the fluctuation of retrieved pulse length gives. If the number of measurements is increased, this broadening will most likely converge towards 10fs.

Measurement #	FWHM _{Air} [fs]	FWHM _{BK7} [fs]
Average	246^{+4}_{-3}	$259.5^{+10.5}_{-4.5}$

Table 4.2: X-FROG results

Examples of FROG and X-FROG trace is shown in fig. 4.7 alongside each other after noise reduction. Since they are originating from the same laser with only a small difference with regards to each other, they look very alike.

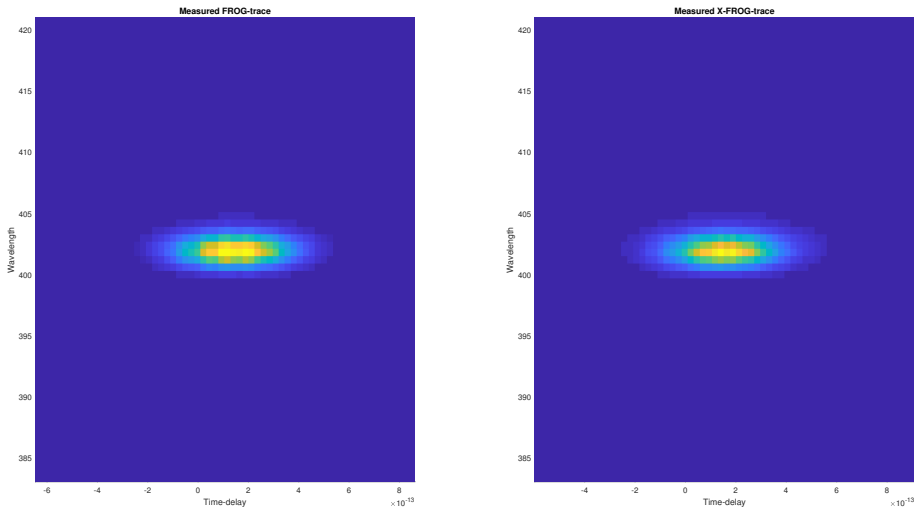


Figure 4.7: Measured FROG and X-FROG traces

Just to check if the algorithm is working as intended it was fed simulated SFG-XFROG traces consisting of either a single chirped pulse or a double pulse with one chirped and one un-chirped peak. In both cases the reference field provided was an un-chirped Gaussian pulse with a temporal width greater than that of the

signal fields. In both cases it solves for the initial field successfully and as such this is further evidence that the X-FROG will function as intended if the source of the erroneous measurements are located. These retrieved simulated fields are shown in fig. 4.8

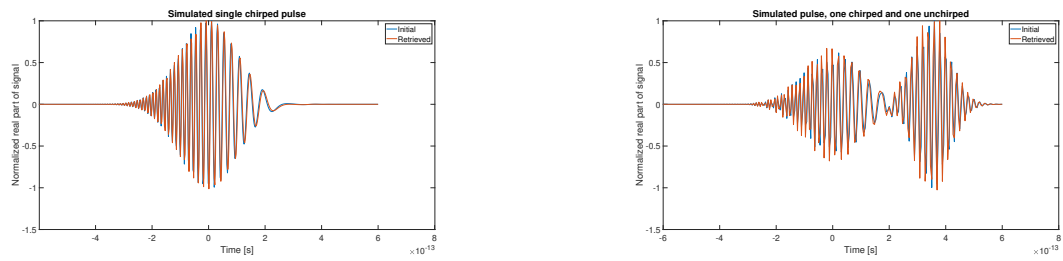


Figure 4.8: Results of X-FROG algorithm provided simulated SFG-XFROG fields

5

Conclusion

The purpose of this thesis was to construct a FROG/XFROG with which the laser physics group at the Royal Institute of Technology could characterise femto-second laser pulses used in and produced in their experiments. Research performed at the laser physics group typically involve broadband pulses so this is yet another constraint on the set-up of it being able to characterise broadband pulses.

The constructed set-up successfully characterises the temporal width of incident laser pulses from a Ti:Sa laser oscillator and is able to perform similar X-FROG measurements by altering one of the incident beams. The phase and spectrum of the pulse however is incorrectly retrieved due to the fact that the measurements are not correct and further investigation into the source of this error needs to be done. Simulations of the algorithm with simulated FROG-traces are successful however and once the source of this error is found it should be functioning as intended.

A number of improvements to the set-up can be performed to increase the characterisation-speed and the performance of the set-up. Two different algorithms are available, the principal components generalised projections algorithm and a ptychographic algorithm. The ptychographic algorithm provides an improved retrieved pulse resolution and requires less densely sampled spectrograms. It converges faster but on today's computers convergence time is no longer an issue.

A re-implementation of the LabVIEW-software is required in order to increase speed. Currently it performs in a 'tic-toc'-manner where the delay-stage moves after which the spectrometer measures. This is repeated until the number of measurements are done. This implementation could instead be replaced with a sweeping approach, where the delay-stage is continuously moving and the integration-time on the spectrometer is low enough to operate under the assumption of the delay-stage position being constant during the measurement. This also seems to be the implementation used in the commercial FROG.

Another improvement is to connect the Matlab-program and the LabVIEW-software so that the measurements are automatically characterised. Currently the user needs to run the result-file from LabVIEW manually in a Matlab-program to characterise pulses.

The last piece of optimisation possible is to optimise the use of space on the optical platform. Replace the parabolic mirror with another one that has a lower focal length as well as obtaining shorter cables for the delay-stage and spectrometer, thus

being able to make it even more compact.

To summarise the work a set-up has been constructed which should be able to fully characterise amplitude and phase of broadband laser pulses. Components have been selected specifically for this reason. Currently it works partly where the temporal width and amplitude of the pulse is retrieved correctly but the bandwidth and chirp is incorrectly measured due to erroneous spectrometer measurements. Once the source of this error has been found the set-up should be operating as intended and the laser physics groups lab should be well equipped for ultrashort pulse characterisation.

Bibliography

- [1] J. Paulo Davim. *Machining : fundamentals and recent advances*. Springer, 2008, pp. 312–313. ISBN: 9781848002128.
- [2] Andrew Marc Weiner. *Ultrafast optics*. Wiley series in pure and applied optics. Hoboken, N.J. : Wiley, c2009., 2009. ISBN: 9780471415398.
- [3] A. Ovsianikov, A. Ostendorf, and B.N. Chichkov. “Three-dimensional photo-fabrication with femtosecond lasers for applications in photonics and biomedicine.” In: *Applied Surface Science* 253.15 (2007), pp. 6599–6602. ISSN: 0169-4332.
- [4] Hui Sun. *Femtosecond-Laser-Assisted LASIK Eye Surgery and Imaging*. Society of Photo-Optical Instrumentation Engineers [SPIE], 2015. ISBN: 9781628416749.
- [5] R. Trebino. *Frequency-resolved optical gating: the measurement of ultrashort laser pulses*. Boston : Kluwer Academic, c2000., 2000. ISBN: 1402070667.
- [6] S. Linden, H. Giessen, and J. Kuhl. “XFROG - A New Method for Amplitude and Phase Characterization of Weak Ultrashort Pulses.” In: *Physica Status Solidi (B)* 206.1 (1998), p. 119. ISSN: 03701972.
- [7] Anne-Lise Viotti et al. “Coherent phase transfer and pulse compression at 1.4 μm in a backward-wave OPO”. QC 20190516.
- [8] Anne-Lise Viotti et al. “Supercontinuum generation and soliton self-compression in $(2) - \text{structuredKTiOPO}_4$.”. In: *Optica* 5.6 (2018), p. 711. ISSN: 23342536.
- [9] Swamp Optics. *Frequently Asked Questions*. <http://www.swampoptics.com/faqs.html>.
- [10] Pablo Londero et al. “Measuring ultrafast pulses in the near-ultraviolet using spectral phase interferometry for direct electric field reconstruction.” In: *Journal of Modern Optics* 50.2 (2003), p. 179. ISSN: 09500340.
- [11] Rana Jafari, Travis Jones, and Rick Trebino. “100% Robust and Fast Algorithm for Second-Harmonic-Generation Frequency-Resolved Optical Gating.” In: *Proceedings of SPIE* 10903 (2018), p. 1. ISSN: 0277786X.
- [12] Rana Jafari and Rick Trebino. “100% Reliable Frequency-Resolved Optical Gating Pulse-Retrieval Algorithmic Approach.” In: (2018).
- [13] T Witting et al. “Time-domain ptychography of over-octave-spanning laser pulses in the single-cycle regime.” In: *Optics Letters* 41.18 (2016), pp. 4218–4221. ISSN: 1539-4794.

- [14] “Measurement of complex supercontinuum light pulses using time domain pychography.” In: (2016).
- [15] Oxford Dictionary. *Laser*. URL: <https://en.oxforddictionaries.com/definition/laser>.
- [16] Claude Rullière. *Femtosecond laser pulses*. Springer, 2005. ISBN: 0387017690.
- [17] Balša Terzić, Cody Reeves, and Geoffrey A. Krafft. “Combining Harmonic Generation and Laser Chirping to Achieve High Spectral Density in Compton Sources.” In: (2015). URL: <http://arxiv.org/abs/1510.03934>.
- [18] Bahaa E. A. Saleh and Malvin Carl Teich. *Fundamentals of photonics*. Hoboken, N.J. : Wiley-Interscience ; Chichester : John Wiley [distributor], c2007., 2007. ISBN: 111858581x.
- [19] *Time-bandwidth Product*. https://www.rp-photonics.com/time_bandwidth_product.html.
- [20] G. P. Agrawal. *Fiber-optic communication systems*. Wiley series in microwave and optical engineering: 222. Wiley, 2010. ISBN: 9780470505113.
- [21] Robert W. Boyd. *Nonlinear optics*. Academic Press, 2008. ISBN: 9780123694706.
- [22] Meijuan Cheng et al. “Large Second-Harmonic Generation and Linear Electro-Optic Effect in Trigonal Selenium and Tellurium.” In: (2019). URL: <http://arxiv.org/abs/1904.01927>.
- [23] Liezun Chen et al. “Bandwidth broadening and spectrum tailoring of second-harmonic generation in transversely nonuniform quasi-phase-matching gratings with spatial spectral dispersion.” In: 126.24 (2015), pp. 5149–5153. ISSN: 0030-4026.
- [24] Robert R. Alfano. *The Supercontinuum Laser Source : The Ultimate White Light*. Springer New York, 2016. ISBN: 9781493933266.
- [25] H. P. Weber. “Method for Pulsewidth Measurement of Ultrashort Light Pulses Generated by Phase-Locked Lasers using Nonlinear Optics.” In: *Journal of Applied Physics* 38.5 (1967), p. 2231. ISSN: 00218979.
- [26] M. Zürch et al. “Characterization of a broadband interferometric autocorrelator for visible light with ultrashort blue laser pulses.” In: *Optics Communications* 321 (2014), pp. 28–31. ISSN: 0030-4018.
- [27] Georgia Institute of Technology - Ultrafast Optics Group : Professor Rick Trebino. *1D-2D-Phase retrieval*. <http://frog.gatech.edu/1d-2d-phase-retrieval.html>.
- [28] R. Trebino, K.W. DeLong, and D.J. Kane. “Using χ^2 to measure the intensity and phase of an ultrashort laser pulse: frequency-resolved optical gating.” In: *Proceedings of LEOS '93* (1993), p. 800. ISSN: 9780780312630.
- [29] O. Melchert et al. “OptFROG - Analytic signal spectrograms with optimized time-frequency resolution.” In: (2018).

-
- [30] Adeline F. Hillier, Claire E. Hillier, and David A. Hillier. “A modified spectrogram with possible application as a visual hearing aid for the deaf.” In: *Journal of the Acoustical Society of America* 144.3 (2018), pp. 1517–1520. ISSN: 00014966.
- [31] Liu Lin-li, Pang Yi, and Hu Zhuang-li. “Application of Spectrogram Analysis in Traditional Vocal Music Teaching and Multimedia Animation Vocal Music Teaching.” In: 11.11 (2016), p. 64. ISSN: 18630383.
- [32] Rick Trebino et al. “Measuring ultrashort laser pulses in the time-frequency domain using frequency-resolved optical..” In: *Review of Scientific Instruments* 68.9 (1997), p. 3277. ISSN: 00346748.
- [33] Takao Yoshinari et al. “Autocorrelation and Frequency-Resolved Optical Gating Measurements Based on the Third Harmonic Generation in a Gaseous Medium.” In: *Applied Sciences (2076-3417)* 5.2 (2015), p. 136. ISSN: 20763417.
- [34] Lina Xu, Erik Zeek, and Rick Trebino. “Simulations of Frequency-Resolved Optical Gating for measuring very complex pulses.” In: *Ultrafast Phenomena Xvi* (2009), p. 941. ISSN: 9783540959458.
- [35] Rick Trebino. “GRENOUILLE measures spatio-temporal distortions.” In: *Laser Focus World* 41.3 (2005), pp. 65–70. ISSN: 10438092.
- [36] S. Linden, H. Giessen, and J. Kuhl. “DFG XFROG. A new method for characterizing weak blue ultrashort pulses.” In: *Technical Digest Summaries of papers presented at the Conference on Lasers & Electro-Optics Postconference Edition CLEO '99 Conference on Lasers & Electro-Optics (IEEE Cat No99CH37013)* (1999), p. 505. ISSN: 9781557525956.
- [37] Benoît Mahieu et al. “Spectral-phase interferometry for direct electric-field reconstruction applied to seeded extreme-ultraviolet free-electron lasers.” In: (2015).
- [38] Alexander M Heidt et al. “Improved retrieval of complex supercontinuum pulses from XFROG traces using a ptychographic algorithm.” In: *Optics Letters* 41.21 (2016), pp. 4903–4906. ISSN: 1539-4794.
- [39] *PRODUCTS / FROGscan*. <https://www.mesaphotonics.com/products-2/pulse-measurement/frogscan/>.
- [40] *Tsunami ULTRAFast Ti:SAPPHIRE OSCILLATORS*. <https://www.spectra-physics.com/products/ultrafast-lasers/tsunami>.
- [41] *Thorlabs website*. <https://www.thorlabs.com/>.
- [42] *Valdas Pasiskevicius*. Personal communication.
- [43] Dirk-Mathys Spangenberg et al. “All optical implementation of a time-domain ptychographic pulse reconstruction set-up.” In: (2016).
- [44] *AvaSpec-Mini2048CL*. <https://www.avantes.com/products/spectrometers/compactline/item/1236-avaspec-mini-cl>.
- [45] *Preconfigured AvaSpec-Mini MK-II*. <https://www.avantes.com/products/spectrometers/compactline/item/1262-avaspec-mini-precon>.

- [46] *LabVIEW*. <http://www.ni.com/sv-se/shop/labview.html>.
- [47] Atsushi Yabushita, Takao Fuji, and Takayoshi Kobayashi. “SHG FROG and XFROG methods for phase/intensity characterization of pulses propagated through an absorptive optical medium.” In: *Optics Communications* 198.1 (2001), pp. 227–232. ISSN: 0030-4018.
- [48] D.J. Kane. “Real-time measurement of ultrashort laser pulses using principal component generalized projections.” In: *IEEE Journal of Selected Topics in Quantum Electronics* 4.2 (1998), p. 278. ISSN: 1077260X.
- [49] Robert A. Adams and Christopher Essex. *Calculus : a complete course*. Pearson Addison Wesley, 2017. ISBN: 9780134154367.

A

Appendix 1

A.1 LabVIEW program

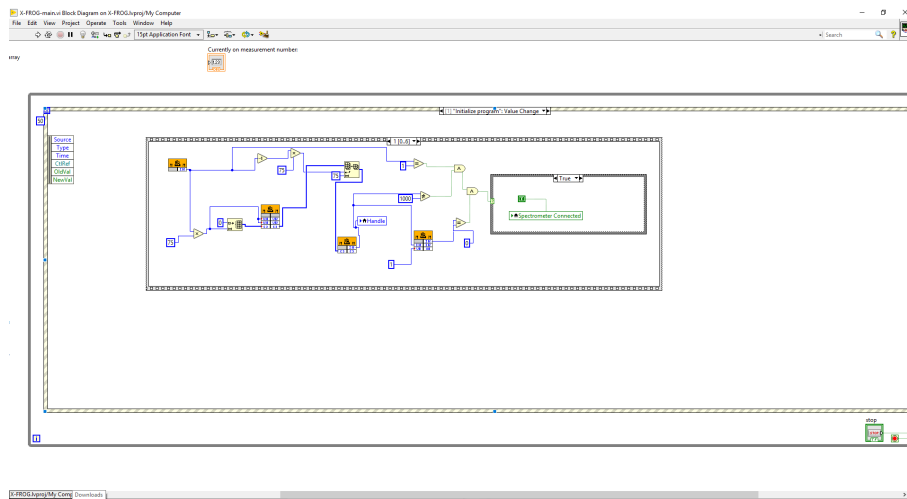


Figure A.1: Establishing of spectrometer connection

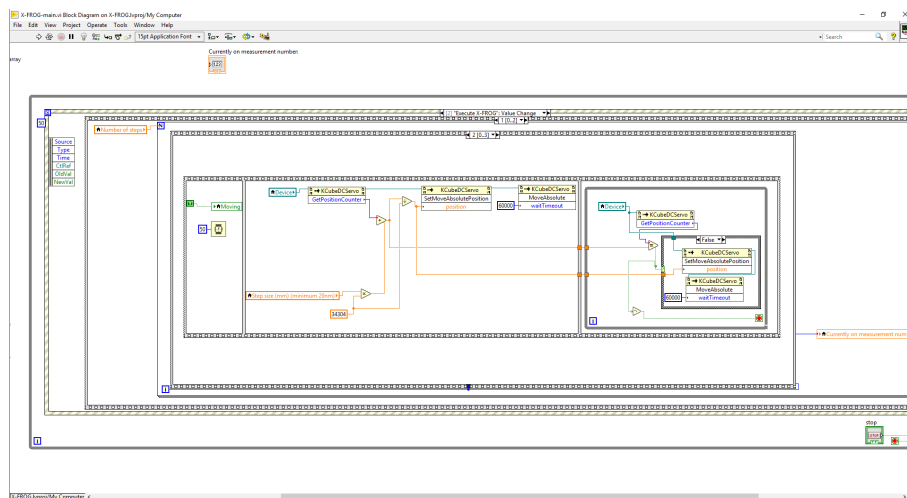


Figure A.2: Updating delay-stage position

A.2 Matlab-code

A.2.1 FROG-trace simulation

```

1 function [intensity , complex] = FROG(signal , gate , version)
2 %FROG Creates SHG FROG/X-FROG-traces from given signals.
3 if strcmp(version , 'frog')
4     outer = signal*(gate. '); % + gate*(guess ');
5     N=length(outer);
6
7     % create the time-delay
8     for i=2:N
9         outer(i,:) = circshift(outer(i,:), [0 1-i]);
10    end
11    outer = fliplr(fftshift(outer , 2));
12    % fft it and re-center.
13    complex = circshift(fft(outer , [], 1) , ceil(N/2)-1);
14    intensity = abs(complex).^2;
15
16 elseif strcmp(version , 'x-frog')
17
18     outer = signal*(gate. ');
19     N = length(outer(:,1));
20
21     for i = 2:1:N
22         outer(i,:) = circshift(outer(i,:), [0 1-i]);
23     end
24     outer = fliplr(fftshift(outer , 2));
25     % fft it and re-center.
26     complex = circshift(fft(outer , [], 1) , ceil(N/2)-1);
27     intensity = abs(complex).^2;
28 else
29     disp('Wrong version-parameter given to frog-function ');
30     intensity = 1;
31     complex = 1;
32 end
33 end

```

A.2.2 UNFROG - returns trace to outer product

```

1 function outer_product = UNFROG(field)
2 %UNFROG takes new frog-trace and unwraps it into the outer
   product matrix
3 %again. Basically FROG-function in reverse.

```



```

4 N = length(field(:,1));
5 outer_product = ifft(circshift(field, 1-ceil(N/2)), [], 1);
6 outer_product = fftshift(fliplr(outer_product), 2);
7
8 for n=2:N
9     outer_product(n,:) = circshift(outer_product(n,:), [0, n
10         -1]);
11
12 end

```

A.2.3 INTENSITY-REPLACE - applies intensity constraint

```

1 function [abs1, compl1] = INTENSITY_REPLACE(int, compl, field
2     )
3 %INTENSITY_REPLACE replaces intensity on simulated trace
4   with that of the
5   %measured trace. I.e it performs the intensity constraint.
6   % int = Intensity of simulated trace
7   % compl = complex simulated trac
8   % field = measured field.
9 int(int==0) = NaN;
10 compl = compl.*(sqrt(field./int));
11 compl(isnan(int)) = 0;
12 compl1 = compl;
13 abs1 = abs(compl1).^2;
14 end

```

A.2.4 GET-TRACE - accepts LabVIEW results file and returns spectrogram

```

1 function [FROG_TRACE, timevector, desired_lambda] =
2     GET_TRACE(delays, lambdas, measurements)
3 %GET_TRACE takes vectors from LabVIEW-program and returns
4   spectrogram along
5   %with vectors containing lambdas and timevector.
6
7 % zero out the 800nm leakage just to get it out of the way
8 measurements(1000:1200,:) = 0;
9 length_vector = length(delays(1,:));
10

```

```

11 % Find position in the file of the maximum value (should be
    zero delay
12 % position.
13 [val, idx] = max(measurements(:));
14 [max_row, max_col] = ind2sub(size(measurements), idx);
15
16
17 % Cut out this section and then center it around the 0 delay
    -axis.
18 FROG_TRACE = circshift(measurements(max_row-length_vector
    /2+1:max_row+length_vector/2, :), [0 -max_col-
    length_vector/2]); %
19 % The wavelengths corresponding to our section
20 lambdas1 = lambdas(max_row-length_vector/2+1:max_row+
    length_vector/2, :);
21
22 % Create new vectors for lambda and steps to interpolate
    with. Same start
23 % and end as before, just evenly spaced points.
24 desired_lambda = linspace(min(min(lambdas1)), max(max(
    lambdas1)), length_vector);
25 desired_step = linspace(min(min(delays)), max(max(delays)),
    length_vector);
26 % Interpolate.
27 for i=1:length_vector
28     FROG_TRACE(:, i) = interp1(lambdas1(:, i), FROG_TRACE(:, i)
    , desired_lambda. ');
29     FROG_TRACE(i, :) = interp1(delays(i, :), FROG_TRACE(i, :),
    desired_step);
30 end
31 for i = 1:length_vector
32
33 end
34
35 % Create the timevector.
36 steps = (desired_step - desired_step(max_col))*2;
37 timevector = steps.*10.^-3./(3e8);
38
39 end

```

A.2.5 GET-PARAMS - accepts pulse as input and returns chirp, bandwidth and tbp

```

1 function [chirp, bandwidth, tbp] = GET_PARAMS(pulse,
    timevector, width, lower, upper)

```

```

2 %GET_PARAMS returns chirp, bandwidth and tbp for pulse
3 % pulse = complex pulse field
4 % timevector = vector with time-indices
5 % width = width of pulse (fs)
6 % Upper and lower are integers representing the position
   indices in pulse
7 % vector where pulse starts and stops, phase is unstable
   outside of this
8 % region (where pulse = 0)
9 phase_val = unwrap(angle(pulse));
10 timevector = timevector;
11 size = length(pulse);
12
13 P = polyfit(timevector(lower:upper), phase_val(lower:upper),
   2);
14
15
16 T_0 = width/1.665;
17 chirp = 0.5*P(1)*((width/1.18)^2);
18 bandwidth = 0.44/width*sqrt(1+chirp^2);
19 tbp = width*bandwidth;
20
21 end

```

A.2.6 PCGPA - principal components generalized projections algorithm

```

1 function [extracted, trace] = PCGPA(field, guess,
   max_iterations, max_error, reference, time, variant)
2 %PCGPA Computes the principal components generalized
   projections algorithm.
3
4 %Functions for normalizing and rescaling traces.
5 normalize_trace = @(field)(field/max(max(field)));
6 scalingfactor = @(Fm, Fr) sum(sum(Fm.*Fr))/sum(sum(Fr.^2));
7
8 field = normalize_trace(field);
9
10
11 plot_distance = 300;
12
13 if strcmp(variant, 'frog')
14     [inten, compl] = FROG(guess, guess, 'frog');
15     inten = inten * scalingfactor(field, inten);
16

```

```

17     iter = 1;
18     error = sqrt((1/length(field)).^2.*(sum(sum(field -
19         inten)).^2));
20
21
22     figure(4)
23     subplot(2,2,1);
24     imagesc(field);
25     subplot(2,2,2);
26     imagesc(inten);
27
28     errors = zeros(10,1);
29     errors(1) = error;
30
31     while (error >= max_error) && (iter <= max_iterations)%
32         && sum(abs(diff(errors))) > 1e-9
33         if mod(iter, plot_distance) == 0 || plot_distance ==
34             1
35             figure(4)
36             subplot(2,2,2);
37             imagesc(inten);
38         end
39
40         [inten, compl] = INTENSITY_REPLACE(inten, compl,
41             field);
42         outer_product = UNFROG(compl);
43         guess = outer_product * outer_product' * guess;
44         guess = guess ./ norm(guess);
45
46         if mod(iter, plot_distance) == 0 | plot_distance == 1
47             [~, idx] = max(abs(guess));
48             guess = circshift(guess, length(guess)/2-idx);
49
50             figure(4);
51             subplot(2,1,2);
52             yyaxis left
53             plot(time, abs(guess./max(max(abs(guess)))));
54             yyaxis right
55             plot(time, unwrap(angle(guess) + pi));
56
57         end
58

```

```

59     [inten , compl] = FROG(guess , guess , 'frog ');
60     inten = inten * scalingfactor(field , inten);
61     error = sqrt((1/length(field)).^2.*(sum(sum(field -
62         inten)).^2));
63
64     disp(['Iteration ' num2str(iter) ' error = ' num2str
65         (error) ' NaN = ' num2str(sum(sum(isnan(field+
66         inten))))]);
67
68     iter = iter+1;
69     errors(2:end) = errors(1:end-1);
70     errors(1) = error;
71 end
72
73 [~, idx] = max(abs(guess));
74 guess = circshift(guess , length(guess)/2-idx);
75
76 extracted = guess;
77 trace = inten;
78 elseif strcmp(variant , 'x-frog ')
79     [inten , compl] = FROG(guess , reference , 'x-frog ');
80     inten = inten * scalingfactor(field , inten);
81
82     iter = 1;
83     error = rmsdiff(field , inten);
84
85 figure(4)
86 subplot(2,2,1);
87 imagesc(field);
88 subplot(2,2,2);
89 imagesc(inten);
90
91 errors = zeros(10,1);
92 errors(1) = error;
93
94 while (error >= max_error) && (iter <= max_iterations)%
95     && sum(abs(diff(errors))) > 1e-9
96     if mod(iter , plot_distance) == 0 || plot_distance ==
97         1
98         figure(4)
99         subplot(2,2,2);
100        imagesc(inten);
101    end

```

```

100     [inten , compl] = INTENSITY_REPLACE(inten , compl ,
101         field);
102     figure(4)
103     subplot(2,2,2);
104     outer_product = UNFROG(compl);
105     guess=outer_product*outer_product'*guess;
106
107     guess = guess./norm(guess);
108
109     if mod(iter , plot_distance) == 0 | plot_distance == 1
110
111         figure(4);
112         subplot(2,1,2);
113         yyaxis left
114         plot(time , abs(guess./max(max(abs(guess)))));
115         yyaxis right
116         plot(time , angle(guess) + pi);
117         axis([min(time) max(time) 0 6.5])
118
119     end
120
121     [inten , compl] = FROG(guess , reference , 'x-frog');
122     inten = inten * scalingfactor(field , inten);
123     error = rmsdiff(field , inten);
124
125     disp(['Iteration ' num2str(iter) ' error = ' num2str
126         (error) ' NaN = ' num2str(sum(sum(isnan(field+
127         inten))))]);
128
129     iter = iter+1;
130     errors(2:end) = errors(1:end-1);
131     errors(1) = error;
132
133     end
134     [~, idx] = max(abs(guess));
135     guess = circshift(guess , length(guess)/2-idx);
136
137     extracted = guess;
138     trace = inten;
139 else
140     disp('Wrong "variant"-paramter given. Should be either "
141         frog" or "x-frog"');
142 end
143 end

```